# A Review on Binderless Tungsten Carbide: Development and Application

Jialin Sun[1] ✉, Jun Zhao[2], Zhifu Huang[1] ✉, Ke Yan[3] ✉, Xuehui Shen[4], Jiandong Xing[1], Yimin Gao[1], Yongxin Jian[1], Hejie Yang[1], Bo Li[1]

✉ Jialin Sun, jialinsun@xjtu.edu.cn; Zhifu Huang, hzf@xjtu.edu.cn; Ke Yan, yanke@mail.xjtu.edu.cn

[1] State Key Laboratory for Mechanical Behavior of Materials, School of Materials Science and Engineering, Xi'an Jiaotong University, Xi'an 710049, People's Republic of China

[2] Key Laboratory of High Efficiency and Clean Mechanical Manufacture of MOE, School of Mechanical Engineering, Shandong University, Jinan 250061, People's Republic of China

[3] Key Laboratory of Education Ministry for Modern Design and Rotor-Bearing System, Xi'an Jiaotong University, Xi'an 710049, People's Republic of China

[4] School of Mechanical and Automotive Engineering, Qilu University of Technology, Jinan 250353, People's Republic of China

HIGHLIGHTS

- Establish processing-composition-microstructure-property relationships governing binderless tungsten carbide (BTC).

- Highlight the densification improving strategies and toughening methods for BTC.

- Provide key challenges as well as the outlook for superior peformance associated with BTC.

ABSTRACT WC-Co alloys have enjoyed great practical significance owing to their excellent properties during the past decades. Despite the advantages, however, recently there have been concerns about the challenges associated with the use of Co, i.e. price instability, toxicity and properties degeneration, which necessitates the fabrication of binderless tungsten carbide (BTC). On the other hand, BTC or BTC composites, none of them, to date has been commercialized and produced on an industrial scale, but only used to a limited extent for specialized applications, such as mechanical seals undergoing high burthen as well as high temperature electrical contacts. There are two challenges in developing BTC: fully densifying the sintered body together with achieving a high toughness. Thus, this review applies towards comprehensively

summarize the current knowledge of sintering behavior, microstructure, and mechanical properties of BTC, highlighting the densification improving strategies as well as toughening methods, so as to provide reference for those who would like to enhance the performance of BTC with better reliability advancing them to further wide applications and prepare the material in a way that is environment friendly, harmless to human health and low in production cost. This paper shows that the fabrication of highly dense and high-performance BTC is economically and technically feasible. The properties of BTC can be tailored by judiciously selecting the chemical composition coupled with taking into careful account the effects of processing techniques and parameters.
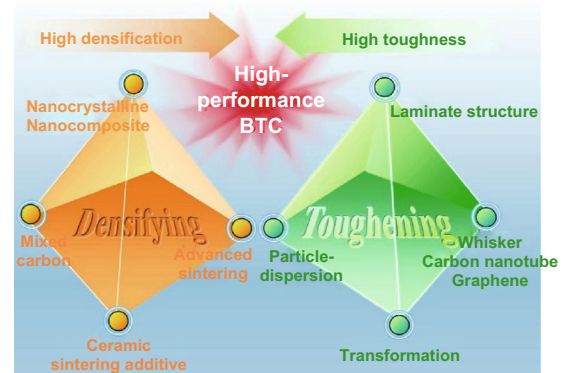
KEYWORDS Binderless tungsten carbide; Sintering; Densification; Toughening; Mechanical properties

1 Introduction

Cemented carbides enjoy great practical significance and have been extensively applied as rock drill buttons, pressing dies, cutting tools, and other abrasion-resistant engineering parts due to their combinations of considerable toughness, strength, and wear resistance [1–5]. The tungsten carbide phase endows the alloy excellent hardness as well as superior wear resistance, while the binder phase is responsible for strength and toughness of the composite materials.

Cobalt (Co) is the mostly employed binder phase during the conventional sintering process due to a combination of fundamental synergistic reasons including its favorable wettability on tungsten carbide, interfacial bonding strength between WC and Co, the plasticity of Co phase in the composite, and its own strength and wear resistance [6, 7]. However, its usage yields the deteriorations in hardness and oxidation/corrosion resistance along with elevated temperature performance owing to the inferior chemical characteristics of cobalt to the carbide phase. Furthermore, thermal stress is ease of generation because of the thermal expansion coefficients misfit [8–10]. When machining metal with high plasticity as pure iron using conventional WC–Co cemented carbide, chip tends to adhere on the rake face of cutting tool, resulting in serious adhesive wear due to the existence of cobalt with low melting point. This issue is exacerbated when cobalt resources may face depletion and economic crises for cobalt occurred because of the excessive development for growing application of cobalt for rechargeable accumulators (batteries) and in superalloys for high-performance jet turbines as illustrated in Table 1 [11]. Additionally, the acute pulmonary toxicity including on macrophage toxicity of WC and Co mixture has been proved to be higher than that of single WC and Co, making sintered WC–Co cemented carbides classified as carcinogenic to humans by International Agency for Research on Cancer (IARC) [12, 13].

On account of the reason above, considerable studies have paid overwhelming attention to the development of BTC. As pioneered by Kanemitsu [14] in 1982, BTC, also named binderless cemented carbide, is tungsten carbide free of any metallic binder including cobalt, iron, and nickel. As shown in Fig. 1, because of the absence of metal binder, BTC composites, possessing attractive properties as exceptional hardness as well as excellent wear/corrosion/oxidation resistance, can be fascinating materials serving in extremely tough environments. However, while initially appealing, none of them, to date, has been commercialized and produced on an industrial or commercial scale. BTCs are only used to a limited extent for specialized applications, such as mechanical seals undergoing high burthen, optical glass lens molds, nozzles for abrasive water jet as well as high-temperature electrical contacts. The production of high-performance BTC is even more challenging. The bottleneck lies in the difficulties encountered in consolidating and toughening BTC. More precisely, it is difficult to consolidate pure tungsten carbide to a full density through conventional sintering, due to its strong energy covalent chemical bonds and high melting point together with low self-diffusion coefficients. Furthermore, WC abnormal grain growth and the formation of sub-carbide W_2C are also unavoidable. As a consequence, BTC composites usually exhibit such disadvantages such as unsatisfactory flexural strength and fracture toughness. In the backdrop of this problem, the development of BTC demands material design solving the twin problems of densification and brittleness.

Table 1 Overview of different uses of cobalt [11]

Product group	Form	Fraction of supply (%)	Trend in use and since when	Recycling	Value added to product
Super-alloys	Metallic	22	Increases 1995	Yes	High
Cutting tools	Metallic	11	Increases 1960	Partly	Medium
Magnets	Metallic	12	Increases 1990	Partly	High
Other applications	Metallic	11	Constant -	No	Low
Batteries	Chemical	22	Increases 2000	Yes	Medium
Chemicals, catalyst	Chemical	9	Increases 1960	No	Low
Resins, pigments	Chemical	13	Constant -	No	Low
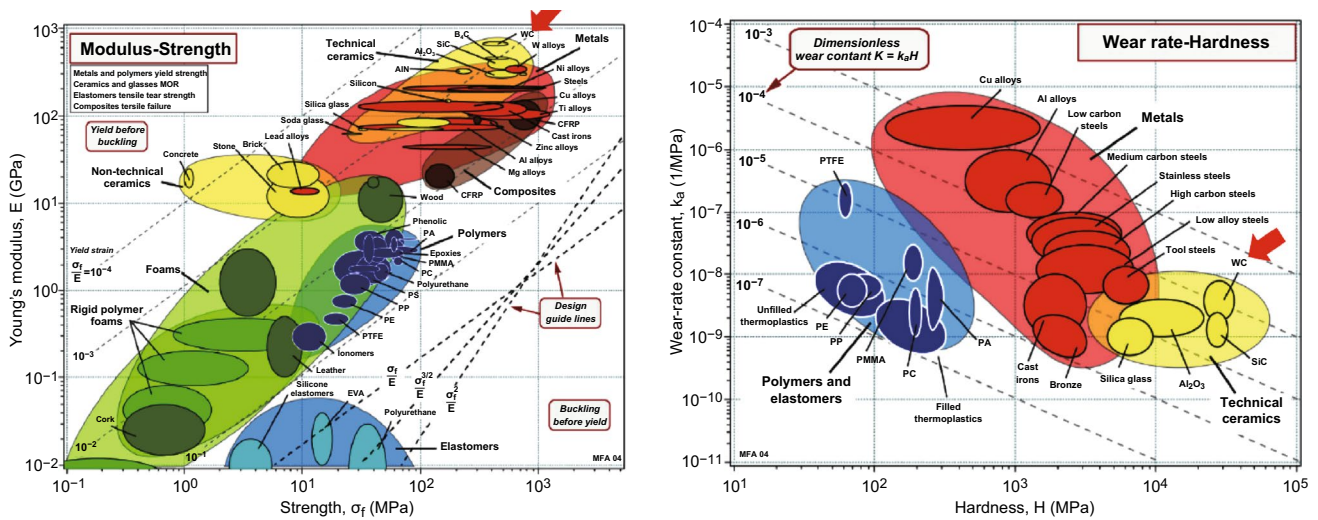
Fig. 1 Ashby diagrams for materials. Left: Young's modulus versus strength, right: wear-rate constant versus hardness. The red arrows point to tungsten carbides [15]. Figure panels reproduced from Ref. [15] with permission from Michael F. Ashby copyright 2009. (Color figure online)

The advanced sintering techniques, such as spark plasma sintering (SPS), reactive spark plasma sintering (RSPS), high-frequency induction-heated sintering (HFIHS) as well as pulsed current active sintering (PCAS), are successfully employed in laboratory scale preparing dense BTC. Particularly, SPS is currently the most applied sintering methods to consolidate BTC or BTC composites. Besides, some sintering additive may act as carbide binder (TiC, TaC, and SiC) or oxide binder (Al_2O_3, ZrO_2, and Y_2O_3), which significantly improve the sinterability of tungsten carbide. On the other hand, with a deep understanding of brittle fracture, various toughening methods, for example transformation toughening, have been proposed to reduce the brittleness and enhance the strength and toughness of BTC.

Though BTC has been developed in various research groups during the past decades, there are still no comprehensive reviews of the processing–composition–microstructure–property relationships governing the material. In light of this, the present article aims to understand the fundamentals of sintering, toughening, and mechanical properties of BTC through a comprehensive review and a systematic examination of the processing, composition, microstructure, and mechanical properties, so as to provide adequate references for those who want to improve the performance of cemented carbides with better reliability and prepare the material in a way that is cost-effective, environmentally friendly, and benign to human health. The following review

will be divided into three major sections: methods improving the sinterability of BTC including the design of mixed carbon content, chemical composition as well as advanced sintering techniques; strategies of toughening BTCs including particle dispersion toughening, transformation toughening, whisker toughening, carbon nanotube toughening, graphene toughening, and laminated structure toughening together with synergistic toughening; and mechanical properties of BTC including hardness versus fracture toughness coupled with wear resistance.

2 Densification of Binderless Tungsten Carbide

Full densification is a prerequisite for BTC achieving its intrinsic properties. However, BTC, owing to the absence of any metallic binders, cannot be prepared by classical liquid-phase sintering but consolidated through solid-state sintering with higher temperature, i.e., above 1800 °C, as well as external pressure because of its low self-diffusion coefficients and strong covalent bonds [16–19]. Thus, it is essential to understand the fundamental of solid-state sintering. Solid-state sintering refers to a diffusional transport of matter through a particular path, which is driven by the reduction in surface free energy of the particle, activated by temperature, and dictated by chemical potential gradients associated with defect concentration in the solid. It can

be divided into three stages [20, 21]. The initial stage features interface formation as well as neck growth between primary particles. It ends when the grain begins to growth. The intermediate stage features extensive grain boundary formations. Pores are still connected with each other in this stage. The final stage begins when pores become isolated. This stage features a fast grain growth with slight densification enhancement. Only four mechanisms are operative in solid-state sintering, and those are grain boundary diffusion, surface diffusion, vapor transport, and lattice diffusion [22]. With respect to solid-state sintering of BTC, grain boundary diffusion may play the critical role in the densification process. During the past decades, some efforts have been made to develop new sintering techniques as well as methodologies improving the sinterability of BTC, so as to obtain a fully dense BTC.

In 1957, Agte et al. [23] firstly attempted to fabricate pure WC employing conventional sintering techniques; however, the result was unsatisfactory. In 1990s, the availability of ultra-fine even nanopowders possessing increased surface energy, and some sintering actives shed light on the preparation of BTC through conventional sintering methods. It is revealed that the densification of nanocrystalline WC–Co powder took place mostly in solid state [24], suggesting that cobalt may not act significantly in the densification process of nanocrystalline WC–Co. Richter et al. [25–27] originally reported on the production of completely densified pure WC using vacuum or pressurized gas sintering owing to the utilization of ultra-fine WC starting powder. The author was appreciated by the EPMA Award of Merit for New Materials in the year of 2000 for developing an ultra-fined BTC with high hardness and wear resistance without any or very low amounts of grain growth inhibitor addition [28, 29]. Recently, some fast sintering techniques such as SPS featuring rapid heating and rapid sintering at relatively lower temperature further facilitated the fabrication of BTC. Fully densified BTC with fine grains is ultimately preferred and is critical to maximize properties. In the following, we critically analyze the major challenges involved in the densification of BTC, including various approaches required to overcome the sintering difficulty of BTC, and then effectively utilize the sintering factors to advantage the consolidation of BTC.

2.1 Mixed Carbon Content

Mixed carbon content has been of great concern to manufacturers of cemented carbide components since the 1950s [30, 31]. Adding free carbon into WC can improve the densification process and reduce or eliminate the formation of brittle phase W_2C in samples obtained by SPS at 1800 °C for 6 min under the pressure of 70 MPa as shown in Fig. 2a. It is suggested that carbon addition is required to reduce oxide impurities as passivation layers located on the surface of WC grains and create the unifying phase compositions, ultimately obtaining single-phase WC materials. Gubernat et al. [33, 34] produced dense single-phase WC polycrystals by hot-pressing sintering with carbon addition. It was found that graphite nanolayers were formed on inter-granular boundaries in carbon-added WC sinters, which significantly improved the thermal conductivity of the polycrystals. The thermal conductivity of sintered WC samples without carbon addition was around 100 W/(m deg), whereas that of obtained WC specimens with carbon addition was close to 200 W/(m deg). However, excessive carbon addition can easily lead to the abnormal grain growth (AGG) of WC as well as the formation of graphite phase inducing cavities and pores in the sintered products [16, 35–38] preventing the full densification, implying that strictly controlling carbon content is essential in the design and fabrication of BTC.

As for conventional cemented carbides as WC–Co cemented carbides, there exists a carbon window, carbon content below which η-phase forms, whereas carbon content above which graphite phase precipitates. Unfortunately, no carbon range but only at a critical value carbon content can deleterious eta phase generation and graphite precipitation be avoided with respect to binderless cemented carbides [39]. Zhang et al. [39] synthesized pure WC employing SPS by tailoring carbon addition to the starting powders. In case of WC with an initial powder size of 0.2 μm, the sintered product was a single WC phase only with a 0.4 wt% carbon mixed. WC_{1-x} phase formed regarding mixed carbon content below 0.4 wt%, while free carbon appeared concerning mixed carbon content above 0.4 wt%. The main phase changed into WC_{1-X} and W_2C for samples without carbon addition. The authors stated that higher mixed carbon content was required for fine-grained BTC with a correct
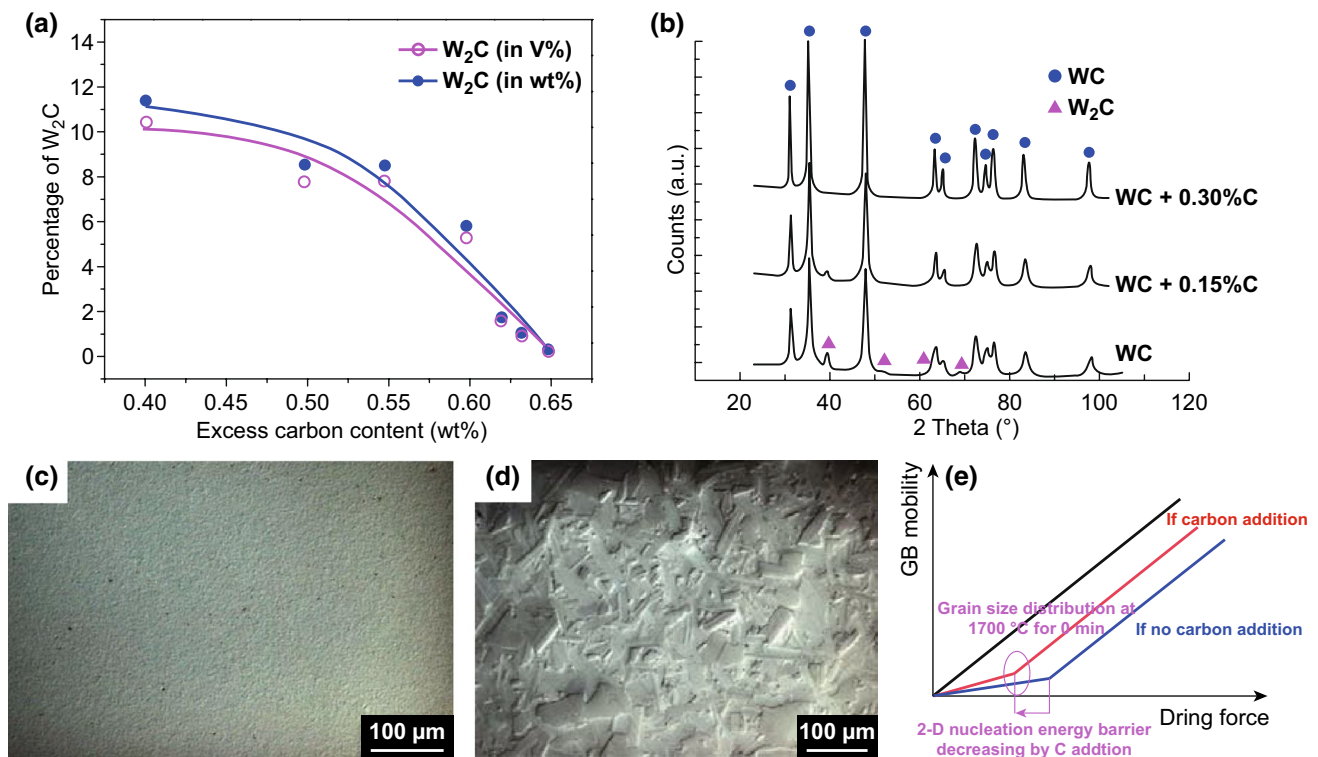
Fig. 2 a Percentage of impurity phase W_2C phase in sintered sample obtained by SPS at 1800 °C for 6 min under the pressure of 70 MPa as a function of C addition in powders [32]. **b** XRD patterns of WC micro and WC ball milled with carbon addition, **c** WC+0.15%C and **d** WC+0.3%C SPS 2200 °C without holding time [40]. **e** Schematic of abnormal grain growth due to addition of C [41]. Figure panels reproduced from Ref. [32] with permission from Taylor & Francis copyright 2015, Ref. [40] with permission from Elsevier copyright 2008, Ref. [41] with permission from Elsevier copyright 2003

phase in comparison with conventional cemented carbides as WC–Co. For one thing, more oxygen was absorbed by WC powders with fine grade (with larger-surface-to-volume ratio). Besides, higher sintering temperature (about 1800 °C) contributed to a complete oxide reduction process. Girardini et al. [40] prepared WC with commercially available micro-WC powders employing SPS with a sintering temperature of 2200 °C and no holding time. With 0.15 wt% carbon addition, the sintered samples appeared no AGG (Fig. 2c), but the W_2C phase was detected as shown in Fig. 2b, implying that the added carbon was insufficiently used for complete oxide reduction. With 0.3 wt% carbon addition, the W_2C phase was avoided (Fig. 2b); however, no improved mechanical properties were obtained as a result of the occurrence of AGG as illustrated in Fig. 2d. Single-phase WC products can be obtained through adding carbon, but AGG occurred once the carbon content exceeded the stoichiometric amount required for the reduction of oxides. In other words, carbon addition reduces or eliminates the brittle phase W_2C, and
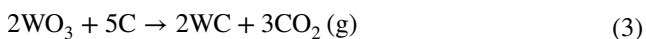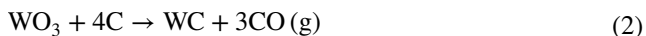
this leads to an enhancement in mechanical properties as fracture toughness; however, at the same time carbon contributes to the AGG and this second effect depresses the mechanical properties as hardness and flexural strength of the material.

As for this, the densification and grain growth behavior of binderless WC are sensitively dependent on the C content within WC. It is rather challenging to strictly control the carbon content during the fabricating process, and the correlation between carbon content and AGG must be carefully taken into account for the design and fabrication of BTC.
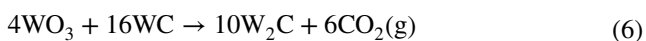
Cha et al. [41] reported that W_2C formation was attributed to the carbon loss through interaction of carbon with surface oxides. Carbon addition was necessary for reduction of oxide impurities located mainly as passivation layers on the surface of WC grains. It is proposed that the densification and grain growth behavior of BTC are sensitively dependent on the C content within tungsten carbide. WC with an initial powder size of 0.57 μm could be sintered to densification by addition

of 0.3 wt% free carbon. The authors also demonstrated the mechanism for carbon addition-induced AGG as shown in Fig. 2e. From their perspective, the carbon addition can not only increase the driving force of grain growth, but also decrease the two-dimensional nucleation energy barrier in WC; as a consequence, the two-dimensional nucleation insufficiently restricts the grain growth due to the sufficiently large driving force for grain growth. Zhao et al. [42] prepared highly dense BTC with a grain size of around 0.4 μm by the SPS method. The authors found that the carbon addition-induced AGG occurred only when the sintering temperature was above 1650 °C. To avoid AGG, specimens were consolidated at a lower temperature 1500 °C with a holding time 5 min, the density was around 99%, and no AGG occurred. On the other hand, based on the well-known equations as Eqs. 1–6, it is suggested that the excess carbon in WC can be moderated by introducing proper contents of WO_3 and W [39, 43].

In the presence of free carbon:

$$W + C \rightarrow WC \tag{1}$$

$$WO_3 + 4C \rightarrow WC + 3CO\,(g) \tag{2}$$

$$2WO_3 + 5C \rightarrow 2WC + 3CO_2\,(g) \tag{3}$$

In the absence of free carbon:

$$W + WC \rightarrow W_2C \tag{4}$$

$$WO_3 + 7WC \rightarrow 4W_2C + 3CO\,(g) \tag{5}$$

$$4WO_3 + 16WC \rightarrow 10W_2C + 6CO_2(g) \tag{6}$$

In summary, carbon control is very essential for BTC achieving maximum densification and performance levels. Strict design of additives including carbon, WO_3, and W together with careful control of thermal processing process is of great importance to the carbon content in the final product.

## 2.2 Nanocrystalline Tungsten Carbide and Its Composites

Based on various sintering models, from the two sphere ones for the initial sintering stage to the microstructural model for the intermediate sintering stage, sintering temperature strongly depends on the grain size, that is, finer initial powder grain size is helpful in lowering the sintering temperature or starting temperature as well as shortening the

sintering process, especially for nanopowders as illustrated in Fig. 3a [44–51]. It is demonstrated that nanosized WC–Co powders start to densify at 600 °C, while submicron-sized powders begin at 1100 °C and regular micro-sized powders at 1320 °C (WC–Co liquidus point) [52–54], conforming the profound effect of grain size on the onset of sintering of WC–Co cemented carbides. Muginstein [55] reported that submicron-sized WC powders begin to densify at 1200 °C, while nanopowders at 500 °C, suggesting that grain size also acted significantly during the sintering of BTC. Furthermore, according to the interfacial energy considerations, there exists a critical pore coordination number, only below which pores will shrink and disappear; otherwise, pores will be stable and not shrink during the sintering process. The grain growth of nanocrystalline particles is helpful in lowering the coordination number of pores and then contributing to the densification process. Also, in general, the average pore size is strongly associated with the average particle size, so nanocrystalline particles may lead to nanosized pores with higher mobility, in turn accelerating the densification process.

Kim [56] and Chvildeev [57, 58] investigated in detail the effect of initial WC particle size on the densification of pure WC by determining the relative densities of sintered BTC with varied initial particle sizes after the same sintering condition. As shown in Fig. 3b, c, the relative density of BTC increased with decreased initial particle size. Therefore, reducing the particles size even down to nanorange is feasible to improve the consolidation process. Girardini et al. [40] compared the densities of micro- and nano-WC with increasing sintering temperature as shown in Fig. 3d. Obviously, there exists a densification delay for micro-WC powder in comparison with nano-WC powder, indicating that nano-WC powder possesses better sintering activity [24, 59–61]. The driving force for densification of WC in general results from a reduction in total surface energy. The internal interface area increased with a decrease in WC grain size, and an enlarged interface area is essential to an enhanced sintering driving force. Based on conventional sintering theories, the sintering driving force can be calculated by Laplace equation (Eq. 7):

$$\sigma = \gamma\left(\frac{1}{R_1} + \frac{1}{R_2}\right) \tag{7}$$

where γ is the surface energy of the material and R_1 and R_2 are the principal radii of the curvature. Obviously,
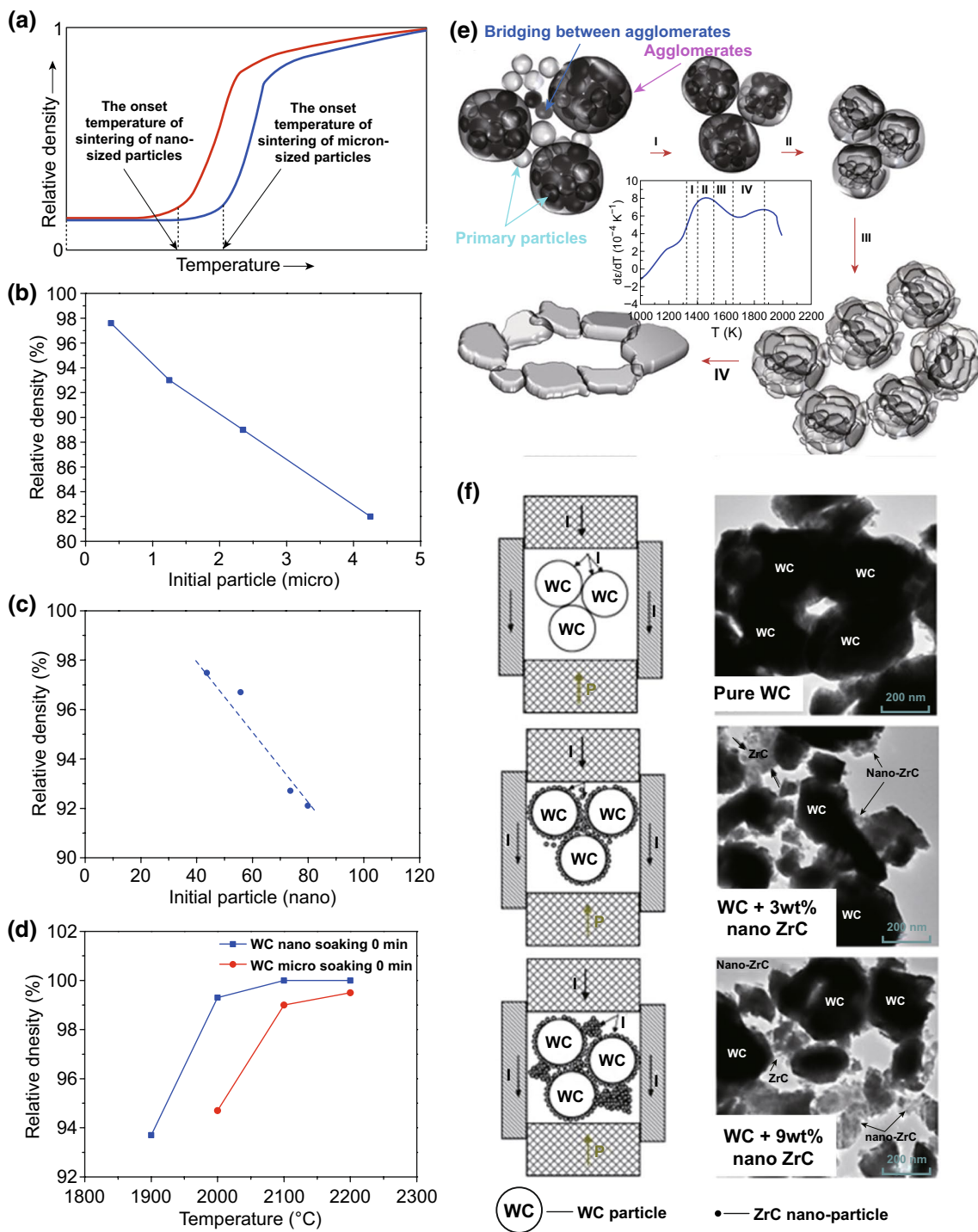
Fig. 3 a Schematic diagram illustrating different onset temperatures of sintering of nano- and micro-sized particles [44]. Relative density of pure WC as a function of initial particle size in BTC **b** microsize [56] and **c** nanosize [57]. **d** Relative density of micro and nano WC versus sintering temperature, without holding time [40]. **e** Schematic of the sintering mechanism of nano WC on the basis of the experimental shrinkage strain rate in a non-isothermal experiment [48]. **f** Schematic diagrams and corresponding TEM micrographs revealing the contact state of WC and ZrC nano-particles during sintering [63]. Figure panels reproduced from Ref. [44] with permission from Taylor & Francis copyright 2008, Ref. [56] with permission from Elsevier copyright 2004, Ref. [57] with permission from Elsevier copyright 2017, Ref. [40] with permission from Elsevier copyright 2008, Ref. [48] with permission from Elsevier copyright 2011, Ref. [63] with permission from Elsevier copyright 2015

nanocrystalline WC powders possess much higher sintering driving forces in comparison with micro-sized ones, due to their superior surface energy. It is concluded that nanocrystalline WC powders possess better sinterability in comparison with micro-sized ones, due to their high surface energy increasing the sintering driving forces.

By investigating sintering kinetics of nanocrystalline WC powders (100–500 nm), Muginstein [62] defined three sintering stages regarding the nanocrystalline WC powder: (1) initial stage, rearrangement of particles at low temperature (850 °C) with no grain or particle growth; (2) intermediate stage, neck formation between powder particles at 1000–1250 °C and initial grain growth at 1200 °C; and (3) final stage, pore elimination accompanied by massive grain growth at 1300–1450 °C.

The sintering kinetics of nano-grained WC was studied in detail by Nanda Kumar et al. [48] using commercially available nano-WC powder without any pretreatment with particle sizes measuring 70 nm (by BET analysis) employing non-isothermal and isothermal sintering. The results illustrated that the agglomeration of nanoparticles was easily to be brought about by surface diffusion resulting in neck growth and grain rotation even at low temperature. The sinterability differences of inter- and intra-agglomerate pore phases introduced substages into the intermediate stage during the sintering process as shown in Fig. 3e. Four substages were defined in the intermediate sintering stage: (1) stage I (~ 80% end density), this stage was located at the end of initial sintering stage/starting of the intermediate sintering stage and covered the temperature from 1027 to 1127 °C. This stage featured a rapid increase in the densification rate, resulting from inter-agglomerate together with intra-agglomerate densification. Most bridges between agglomerates disappeared and then clusters impinged on each other. At the end of this stage, the microstructure evolved into most agglomerate and continuous pore; 2) stage II (~ 83 to 85% end density), this stage was identified for its constant density. The shrinkage, if any, occurred purely as a function of intra-agglomerate densification. At the end of this stage, the microstructure was characterized by well-demarcated agglomerate boundaries; 3) stage III (~ 85% end density), in this stage, the net shrinkage stain rate decreased owing to inter-agglomerate pore stability as well as a small amount of grain growth within agglomerates; (4) stage IV (~ 94% end density), in this stage, because of temperature driven coupled with the reduction in pore coordination number, the

system tried to evolve by massive grain growth within the agglomerates, leading to the breakup of the agglomerate and sintering start of stable inter-agglomerate pores. The pores started to shrink rapidly and surpassed the grain growth rate with the transform of agglomerates into large grains. Thus, in nano-WC system, the grain growth acted to enhance the densification process by changing the pore stability from thermodynamically stable to unstable through decreasing the pore coordination number. Actually, considering the thermodynamics of the sintering process, complete densification cannot be achieved in nano-WC powders without grain growth as one abets the other [48].

Besides reducing the particle size of WC matrix, it is also effective to facilitate the sintering of WC by dispersing some nanosized second-phase additive within micro-sized WC matrix grains or at the grain boundaries of WC matrix. Ren et al. [63] reported that the densification of BTC was significantly improved through adding appropriate amount of ZrC nano-powder. The densification mechanism was that submicron-sized WC particles were surrounded by nanosized ZrC particles through the mixing process as shown in Fig. 3f. WC particles tended to gather together to form a large particle regarding pure WC sample. However, with respect to 3 wt% nano-ZrC-added specimen, submicron-sized WC particles were adhered by nano-ZrC particles (Fig. 3f). The adherent nano-powder filled the inter-space resulting from particle rearrangement and plastic deformation of WC grains and then improved the densification process. On the other hand, nanopowders tended to agglomerate as a result of their high specific surface areas. Considering the WC–9 wt% ZrC samples, the agglomeration of nano-ZrC was serious, consequently leading to the deterioration of densification.

Biswas [64] prepared fully dense WC–6 wt% ZrO_2 composites with the assistance of ZrO_2 powders of 27 nm as second-phase employing SPS (sintering at 1300 °C for holding 5 min). As demonstrated in Table 2, employing the same consolidation technique, sintering temperature required for WC achieving full densification was significantly reduced as a function of nanocrystalline ZrO_2 addition. Furthermore, it should be noted that WC can be consolidated utilizing nano-sized ZrO_2 at a lower temperature 1300 °C in comparison with WC–Co at 1400 °C [65], indicating that nano-ZrO_2 is an ideal alternative to Co binder as sinter additive. The densification improving mechanism was ZrO_2 enhancing

Table 2 Densification data of WC–6 wt% ZrO$_2$ composites and WC–6 wt% Co cemented carbides sintered via spark plasma sintering (SPS)

Material composition	Starting powder size (μm)	Sintering techniques and temperature (°C)	Holding time (min)	Pressure (MPa)	Relative density (%)
WC–6 wt% ZrO$_2$ [64]	0.2	SPS, 1300	5	30	99.9
WC–6 wt% Co [65]	0.2	SPS, 1300	5	30	91.4
WC–6 wt% Co [65]	0.2	SPS, 1400	5	30	100

sintering kinetics as a result of size effect together with high "constriction resistance." Nanosized ZrO$_2$ increased the volume fraction of the interface area due to its higher specific surface area and then resulted in faster mass transport considering grain boundaries providing faster diffusion paths. Nanosized ZrO$_2$ particles enhanced "constriction resistance," because of their nanosize, resulting in higher resistivity coupled with smaller particle-to-particle contact area, based on Eq. 8 [66]:

$$R_c(n, a, l) = \frac{\rho f_s}{2\pi na} \arctan\left(\frac{\sqrt{l^2 - a^2}}{a}\right) \tag{8}$$

where R_c is the constriction resistance, ρ is the resistivity of the powder, a is the linear dimension of the inter-particle contact, f_s is the shape factor, l is the nearest distance between the contacts, and n is approximately the number of squares with sides $2l$. Thus, voltage drop took place over a small distance around the nano-ZrO$_2$ contact area. High-resistance localized area with a rather high Joule heating was formed, resulting in local temperature increase and then a faster mass transport.

2.3 Ceramic Sintering Additive

Sintering additives, which are present in solid state only or may form liquid phases, are intentionally added to control the microstructural and dimensional development during sintering. Numerous researches have demonstrated that minor additions of second phase, which increase the grain boundary diffusion and surface diffusion in this system, accelerate the densification process [67]. Therefore, besides the mixed carbon content and carbide grain size, the design of chemical composition is also a logical strategy to enhance the sinterability of tungsten carbide in conventional methods. The low melting point of the metal and possibility of carbonation and oxidation make the selection of the

transition-metal carbides (TiC [68, 69], TaC [70], and SiC [71, 72]) and metal oxides (Al$_2$O$_3$ [73], ZrO$_2$ [74], Y$_2$O$_3$ [75, 76], and La$_2$O$_3$ [77]) binders more favorable for tailoring the densification process of BTC.

2.3.1 Titanium Carbide (TiC)

Titanium carbide (TiC), with a cubic structure (Ti atoms on one fcc sublattice and C atoms on the other), has been recognized as one of the most significant metal carbides for BTC manufacturing, due to its prominent intrinsic properties, such as high melting point (3067 °C), high thermal conductivity (30×10^6 S cm^{-1}), high hardness (TiC has 31 GPa Vickers hardness and WC has 25 GPa), high elastic modulus (410–450 GPa), high thermodynamic stability together with low friction coefficient and density (4.93 g cm^{-3}) [78]. In 1982, Kanemitsu et al. [15] firstly developed a WC–TiC–TaC binderless cemented carbide. Since then, several researches have been performed to improve the sinterability of tungsten carbide through adding TiC as a carbide binder.

Kim et al. [79] demonstrated the effect of TiC content on the sintering of WC–TiC composites as illustrated in Fig. 4. Initially, all specimens showed volume increases because of the thermal expansion. The onset of shrinkage of pure WC started at about 1200 °C, while that of TiC-added WC composites took place at around 950–1100 °C, suggesting that the content of TiC had a significant influence on the onset of sintering of WC-based composites. Sintering temperature was decreased significantly with the increasing TiC content. As depicted in Fig. 4b, under the same sintering condition, the density of pure WC sample was about 78%, while that of WC–50 at.% specimen was 98.5%. Obviously, TiC was beneficial to enhance the relative density of WC–TiC composites. The densification mechanism was that TiC acted as a carbide binder resulting from the formation of WC–TiC solid solution phase [80–83]. As shown in Fig. 4c, the lattice
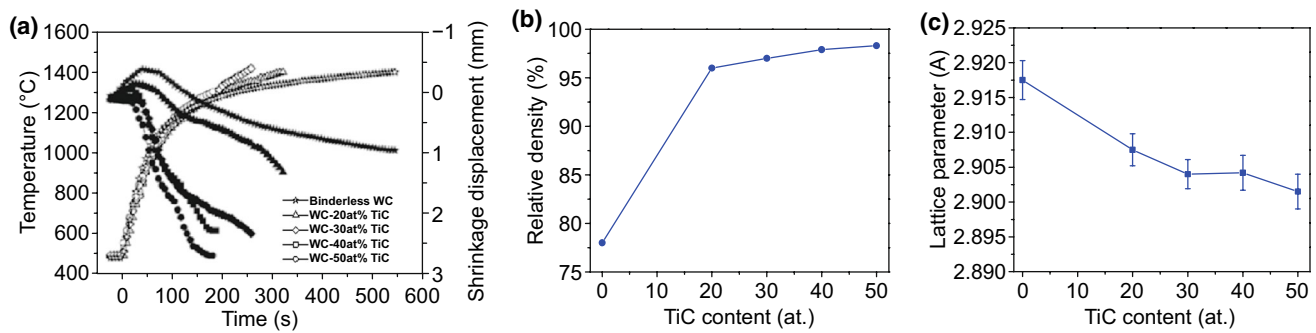
Fig. 4 a Variations of temperature and shrinkage displacement with heating time during high-frequency induction heated sintering of WC–x at.% TiC hard materials (under 60 MPa pressure, 2800A). **b** Relative density as a function of TiC content. **c** Plot of WC phase lattice parameter as a function of TiC content produced by PCAS [79]. Figure panels reproduced from Ref. [79] with permission from Hanyang University copyright 2007

parameter of WC decreased with the increasing contents of TiC addition, confirming the formation of a series of solid solution.

It was thought that the formation of solid solutions between additive and WC could facilitate the densification of WC-based materials. The similar densification mechanism was found in WC–TiC–TaC [80], WC–VC [84], and WC–Mo_2C [85] systems. Imasato et al. [80] reported that the addition of TaC and TiC facilitated the sintering process of WC because of the formation of (W, Ta, Ti) C solution phase. Huang et al. [84] suggested that VC addition facilitated densification as a function of (V, W) C solid solution phase formation, so that full densification for WC–VC composites could be achieved at lower temperature or within shorter sintering time in comparison with pure WC.

2.3.2 Silicon Carbide (SiC)

Silicon carbide (SiC) possesses a high hardness above 20 GPa together with a relatively high Young's modulus 440 GPa. Furthermore, SiC is less expensive than WC. Additionally, SiC is proved to be a toughening phase for many ceramics including WC. So, SiC can be an excellent candidate for improving the sinterability of BTC. It is proposed that the sintering temperature of WC was significantly decreased as a function of SiC powder and/or SiC whiskers addition [86–88].

Dense WC–SiC composites were fabricated by Nino et al. [87] employing hot-pressing sintering methods. As demonstrated in Fig. 5a, no dense sintered body was obtained at 1600 °C for pure WC though hot-pressing applied, indicating

that 1800 °C was essential to realize densification. However, with respect to WC–SiC composites, high relative density above 98% was achieved as a result of 2–10 mol % SiC addition.

As shown in Fig. 5b, WC–SiC_w composites containing 3–5 vol% SiC_w were fully dense at 1650 °C, while pure WC could not be sintered densely at 1650 °C, suggesting that SiC_w was efficacious in lowering the sintering temperature of WC [88]. However, the relative density gradually decreased with the SiC_w addition regarding 10 vol% SiC_w. 1750 °C was necessary for 30 vol% SiC_w composites to realize a fully dense level.

However, while initially appealing, caution should be exercised as the mechanism of the WC sinterability improvement by SiC addition, to data, is still unclear and WC–SiC composites, possessing only a small market share, were employed only to a limited extent for specialized applications. Moreover, it is noted that SiC addition tended to result in the abnormal growth of WC grains; thus, some grain growth inhibitors such as ZrC [71], NbC [72], Mo_2C [89], VC [56], and Cr_3C_2 [86, 90] are required to obtain the excellent microstructure as well as mechanical properties.

2.3.3 Alumina (Al₂O₃)

Alumina (Al_2O_3), as a refractory oxide, has been widely used in industry applications owing to its excellent properties, such as low density, good thermal and chemical stability, high hardness, and high temperature [91]. Besides, the price of Al_2O_3 is lower than that of Co and many other metal oxides as ZrO_2 and MgO. Moreover, Al_2O_3 has a
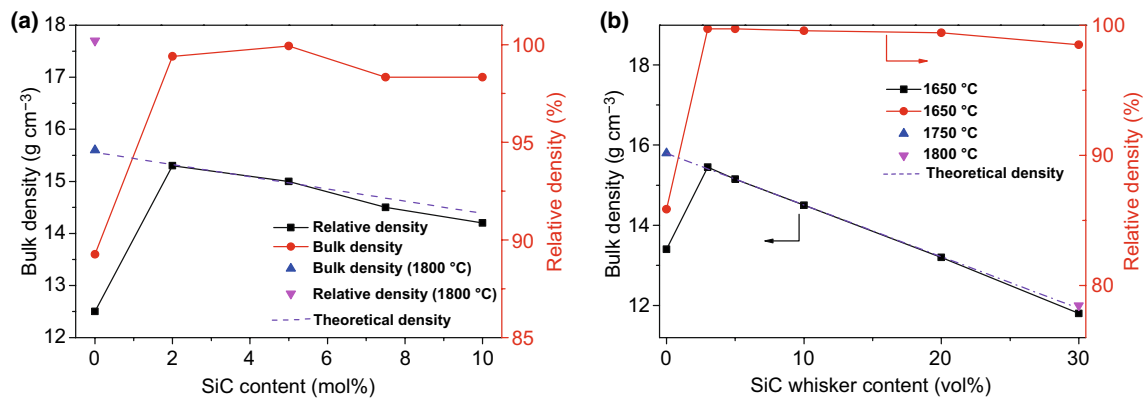
Fig. 5 a Bulk density and relative density of WC–SiC composites [87]. **b** Bulk density and relative density of WC–SiC$_w$ composites [88]. Figure panels reproduced from Ref. [87] with permission from Japan Institute of Metals (JIM) copyright 2011, Ref. [88] with permission from Japan Institute of Metals (JIM) copyright 2008

lower melting point in comparison with that of ZrO$_2$ and MgO, which is more helpful in lowering the temperature of reinforced materials by generating liquid phase. Therefore, Al$_2$O$_3$ can be an economical and suitable candidate to replace Co in WC matrix [92–99].

Zheng et al. [99] investigated the effect of Al$_2$O$_3$ addition on the sintering behavior of WC–Al$_2$O$_3$ composite as shown in Fig. 6a, b. For pure WC, the densification process took place at around 1140 °C and ended at about 1880 °C. As far as WC–3 wt% Al$_2$O$_3$ was concerned, the densification starting point was ~ 930 °C and the ending temperature was ~ 1770 °C. Obviously, Al$_2$O$_3$ addition significantly facilitated the sintering process by accomplishing the densification process at a lower temperature range owing to Al$_2$O$_3$'s lower melting point of around 2050 °C than WC (about 2785 °C), which is well in line with the findings of Oh et al. [100] as depicted in Fig. 6c.

Qu et al. [101] prepared highly dense WC–(10, 20, 30, 40, 50) vol% Al$_2$O$_3$ composites by a hot-pressing sintering method, suggesting that the relative density increased with the increasing content of Al$_2$O$_3$. Furthermore, the author demonstrated that Al$_2$O$_3$ addition was effective to suppress the WC grain growth. A work conducted by Seung-Jin Oh et al. [102] reported the same conclusion through HFIHS methods as demonstrated in Table 3.

2.3.4 Zirconia (ZrO$_2$)

Zirconia (ZrO$_2$) has received attention as a substitute for Co because of its excellent properties: (1) high chemical stability up to quite high temperature about 1400 °C; (2) not softening at elevated temperatures; (3) high electrochemical corrosion resistance; (4) increasing toughness by transformation toughening [103–107]. Besides, ZrO$_2$ was found to facilitate the sintering of BTC by many researches [108–110].

Basu et al. [111] proposed that it was inappropriate to use ZrO$_2$ itself as the sintering additive, but Y$_2$O$_3$-stabilized tetragonal ZrO$_2$ was effective to improve the sinterability of BTC. Figure 7a illustrates the effect of Y$_2$O$_3$ content in ZrO$_2$ on the densification of WC employing pressureless sintering. Though sintered at 1700 °C for 1 h, the composites can only achieve a relative density of 93.9% with Y$_2$O$_3$-free ZrO$_2$ addition, conforming that Y$_2$O$_3$-free ZrO$_2$ was ineffective to enhance the densification process of WC.

Figure 7b, c demonstrates the densification curves for the pure WC sintered at 1800 °C for holding 5 min and the WC3Z (WC–3 wt% ZrO$_2$) and WC10Z (WC–10 wt% ZrO$_2$) samples sintered at 1600 °C for holding 5 min. Caution should be noted that the ZrO$_2$ used in this research was 3 mol % Y$_2$O$_3$-stabilized tetragonal ZrO$_2$. Ignoring several shrinkage rate fluctuations below ~ 650 °C, it is considered that the densification process took place when the shrinkage rate turned to be positive and ended when the shrinkage rate was down to zero again. As shown in Fig. 7b, the densification of pure WC started at around 1050 °C and ended at around 1790 °C. Concerning WC sample, the densification began at a lower temperature ~ 850 °C and ended at a lower temperature ~ 1600 °C in comparison with pure WC. Further increasing ZrO$_2$ content, the densification process can be
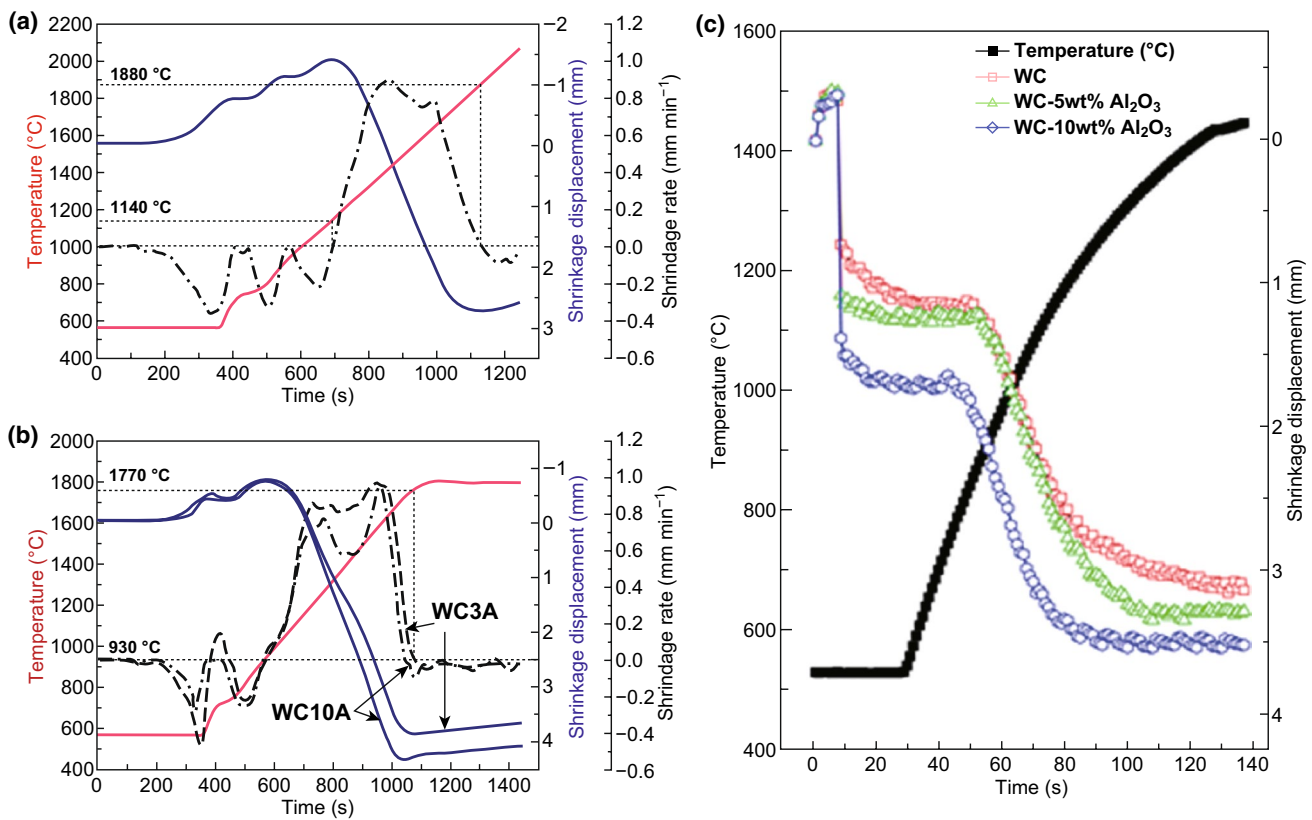
Fig. 6 Densification behavior of **a** WC, SPSed at 2060 °C for 0 min, and **b** WC3A (WC–3 wt% Al$_2$O$_3$) and WC10A (WC–10 wt% Al$_2$O$_3$), SPSed at 1800 °C for 5 min [99]. **c** Variations of temperature and shrinkage with heating time during the pulsed current activated sintering of WC–Al$_2$O$_3$ powder [100]. Figure panels reproduced from Ref. [99] with permission from Elsevier copyright 2012, Ref. [100] with permission from Elsevier copyright 2016

Table 3 Average grain size and relative density of pure WC and WC–Al$_2$O$_3$ composite after the same HFIHS sintering conditions with same staring WC powders [102]

Composition	Relative density (%)	Grain size (nm)
WC	97	265
WC–5 vol% Al$_2$O$_3$	98	185
WC–10 vol% Al$_2$O$_3$	99	138
WC–15 vol% Al$_2$O$_3$	99.8	101

accomplished at even lower temperature range. With respect to WC10Z specimen, the densification beginning temperature yielded at ~ 740 °C, and the ending point of densification was ~ 1530 °C. Obviously, ZrO$_2$ addition significantly improved the densification process of WC. Additionally, the cures exhibited a bimodal shape regarding WC–ZrO$_2$ specimens, an extra shrinkage rate maximum appearing at about 1050–1100 °C, which was considered as a result of

transformation of retained m-ZrO$_2$ in original ZrO$_2$ powders involving a volume decrease (3–5%) and assisting particle rearrangement during the densification process. Since the densification process is mainly diffusion controlled, it is denoted that ZrO$_2$ addition elevated the diffusivity of WC–ZrO$_2$ system. Densification starting temperature was decreased due to ZrO$_2$ addition, so the densification improving mechanism can be concluded that ZrO$_2$ addition lowers the activation energy for atoms diffusion, resulting in a higher diffusivity and then an enhanced densification [104].

2.4 Advanced Sintering Techniques

The properties of BTC fabricated by powder metallurgy can be significantly enhanced through improving the density coupled with decreasing the grain size of the sintered bodies. However, since WC possesses a high melting point (2785 °C) and no metallic binder addition, it is rather
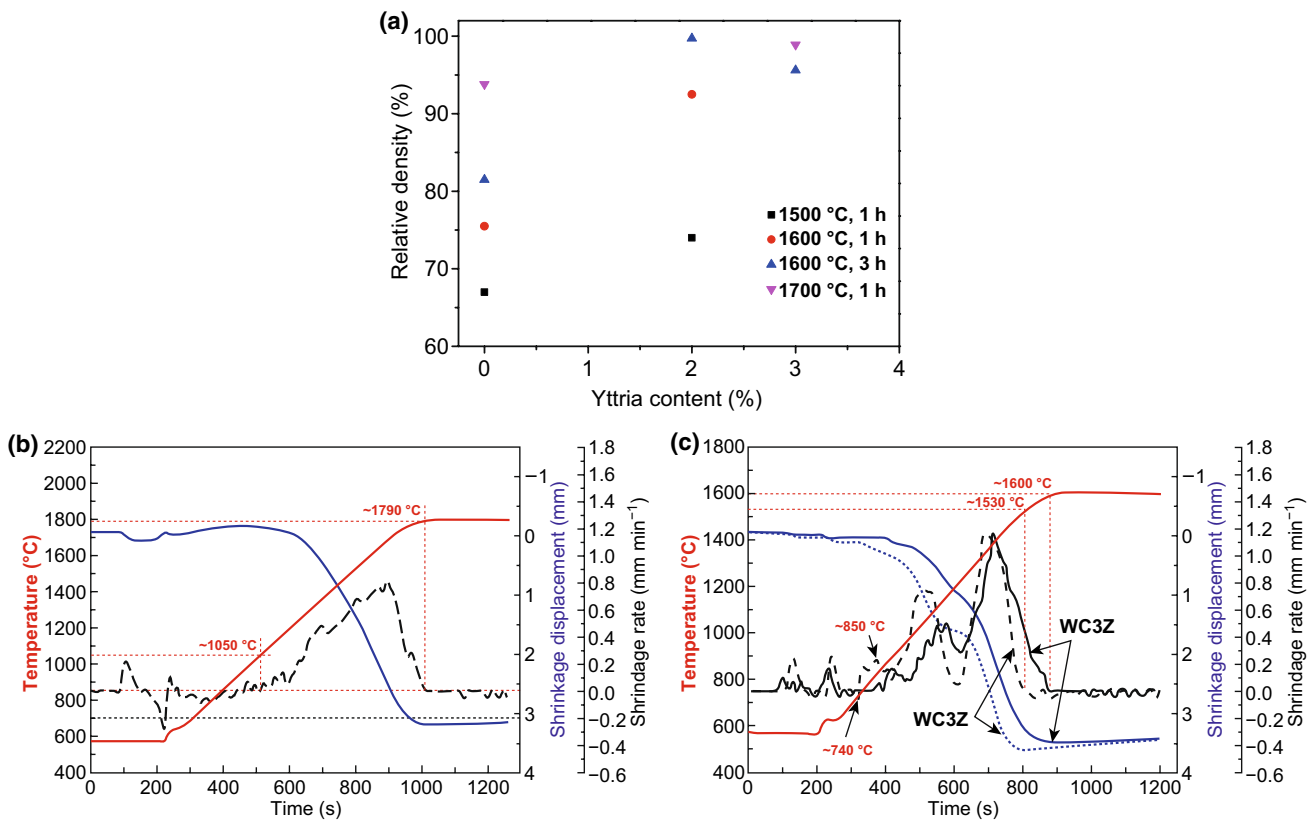
Fig. 7 a Relative density obtained at different sintering temperatures with WC composites with 6 wt% ZrO$_2$ (stabilized with varying amount of Y$_2$O$_3$) sinter-additive [111]. Densification curves for **b** pure WC sintered at 1800 °C for holding 5 min, **c** WC3Z and WC10Z specimens sintered at 1600 °C for holding 5 min [104]. Figure panels reproduced from Ref. [111] with permission from Elsevier copyright 2005, Ref. [104] with permission from Elsevier copyright 2013

difficult to consolidate WC to a high density with a fine grain employing the conventional sintering process. Generally speaking, excessively high sintering temperature and/or long holding time is easy to incur porosities in the sintered material and results in coarsening of the microstructure. Thus, it is crucial to carefully control the sintering parameters, particularly sintering temperature and time, for preparing materials with excellent properties. Compared with conventional sintering techniques, some advanced sintering techniques such as fast sintering techniques are known for their higher heating and cooling rates, as well as shorter densification time at lower sintering temperature, as a function of external field together with high-pressure application such as SPS, RSPS, PCAS, and HFIHS. SPS, for example, applying pulsed electrical fields coupled with resistance heating and pressure as shown in Fig. 8a, can consolidate materials rapidly, uniformly, and thoroughly because of the large pulsed direct current during heat treatment of powders

in the graphite die. The external field is prone to enhancing the mass transport during the sintering, and the effect can be determined through the electromigration theory (Eq. 9) [113]:

$$J_i = -\frac{D_i C_i}{RT}\left[\frac{RT\,\partial ln C_i}{\partial x} + Fz^*E\right] \qquad (9)$$

where J_i is the flux of the diffusing ith species, D_i is the diffusivity of ith species, C_i is the concentration of ith species, F is Faraday's constant, z^* is the effective charge on the diffusing species, E is the field, R is the universal gas, and T is absolute temperature. Furthermore, high pressure is helpful in accelerating the particle rearrangement, sliding, or even distortion as well as breaking (Fig. 8b). These merits of fast sintering techniques highly open up the possibilities for successful production of highly dense BTC with fine grains.

Table 4 summarizes the densification as well as grain sizes of materials obtained through various sintering techniques. Obviously, even without any sintering additive or

(a)

(b)
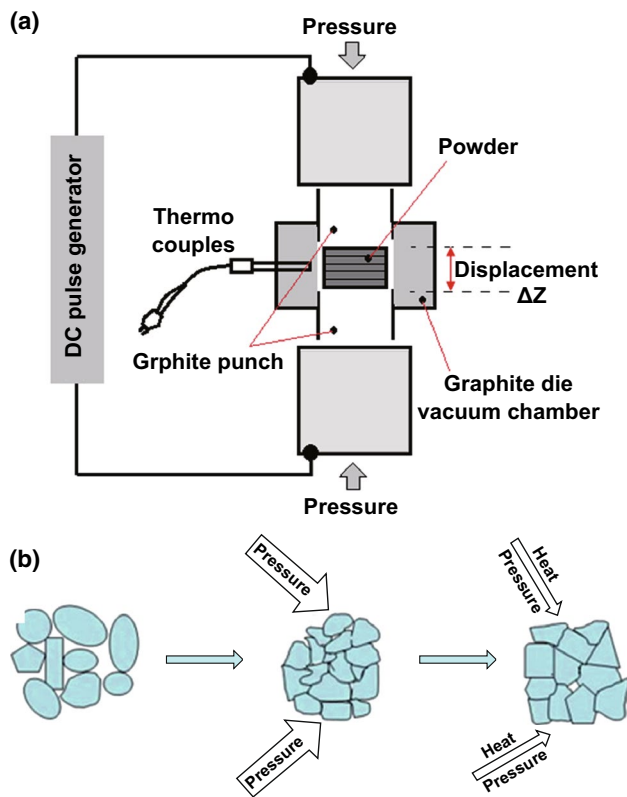
Fig. 8 a Schematic representation of SPS equipment [112]. **b** The formation mechanism of WC sintered under high pressure [18]. Figure panels reproduced from Ref. [112] with permission from Taylor & Francis copyright 2007, Ref. [18] with permission from Elsevier copyright 2016

grain growth inhibitor addition, fine-grained WC with nearly full densification was prepared. SPS, the most employed sintering technique during the fabrication of BTC, attracted most attention among materials researchers as well as production engineers. SPS was proposed according to the idea employing the plasma on electric discharge machine for sintering ceramics and metal in the early 1960s by Inoue et al. [114] expecting that the plasma-assisted sintering could contribute to the realization of advanced materials [115]. Thereafter, the concept obtained further development during the mid-1980s to the early 1990s. In 1998, it was first experimentally verified that SPS enhanced the densification of materials [116]. SPS is also named as pulsed electric current sintering (PECS) or electric pulse-assisted consolidation (EPAC) [117, 118]. Conventional rapid heating can easily result in temperature gradients and then differential densification (non-uniform microstructures), low density, or sample

cracking. SPS densifies the materials at a homogeneous temperature or heat distribution by applying pulsed direct current through the sample and graphite die. Furthermore, it is found by Huang et al. [119] that the grain growth of WC hardly occurred during SPS process, which is greatly different from WC–Co cemented carbides showing obvious WC grain coarsening during SPS process [120].

3 Toughening of Binderless Tungsten Carbide

Brittle fracture limits the use of BTC in many applications. The fracture toughness of BTC strongly depends on the interaction of the crack tip stress field with the microstructure. Therefore, microstructural design to reduce stresses near crack tips has been a key issue during the development of highly tough BTC.

In order to reduce the brittleness and to enhance the strength and the toughness of BTC, varieties of traditional toughening methods, including particle dispersion toughening, transformation toughening, whisker toughening, and synergistic toughening, have been proposed in the past decades. Recently, with our deep understanding of brittle fracture, some new-concept toughening methods, such as laminated structure toughening, carbon nanotube toughening as well as graphene toughening, are proved to be also operative in BTC, offering great promise of a revolutionary advance in the production of high-toughness BTC. The purpose of this section is to demonstrate how the knowledge gained is currently being applied to the development of highly tough BTC or BTC composites.

3.1 Particle Dispersion Toughening

Particle dispersion toughening, as the simplest toughening method, is the foundation of the other toughening methods of ceramics [131]. It can be subdivided into non-transformation secondary-phase particle dispersion toughening, ductile particle dispersion toughening as well as nanoparticle dispersion toughening. The major toughening mechanisms existing particle-toughened ceramics were ascribed to (i) crack deflection by the particulates ahead of a propagating crack (crack deflection model); (ii) crack bridging by particulates (particulate bridging model); (iii) interaction between the crack front and particulates (crack front bowing model);

Table 4 Results of various sintering techniques regarding densification as well as grain size

Sintering process	Temperature and holding time	Heating rate (°C min^{-1})	Pressure (MPa)	Starting powder and grain size	Relative density (%)	Sintered grain size (nm)
HP[a] [33]	2150 °C/1 min	N/A	25	WC, 0.5–0.7 µm	97.5	
HP [121]	2000 °C/30 min	3-10	28	WC–0.33 wt% VC–0.54 wt% Cr_3C_2, 0.53 µm	97.9	730
HIP[b] [121]	1750 °C/120 min	N/A	150	WC–0.33 wt% VC–0.54 wt% Cr_3C_2, 0.53 µm	99.4	750
HP [90]	1600 °C/10 min	50	50	WC–20 mol% SiC, 0.73 µm	98	530
HP [90]	1600 °C/10 min	50	50	WC–20 mol% SiC–0.9 mol% Cr_3C_2, 0.73 µm	98	340
HP [101]	1540 °C/90 min	10	39.6	WC–40 vol% Al_2O_3	97.98	2750
HPHT[c] [18]	1500 °C/20 min	100	5 GPa	WC, 150–250 nm	99.2	150-250
GPS[d] [122]	1860 °C/60 min	3-6	0	WC, 1.03 µm	95.1	
SPS[e] [119]	1500 °C/4 min	180	60	WC, 200 nm	99.6	200
SPS [123]	1460 °C/3 min	150	30	WC–0.1 wt% C, 200 nm	99.5	350
RSPS[f] [124]	1350 °C/1.5 min	100	60	W_2N-C, 40 nm		270
SPS [125]	1800 °C/1 min	150	80	WC, 55 nm	100	160
SPS [126]	1750 °C/10 min	50	50	WC, 1.8 µm	99.6	
SPS [42]	1750 °C/0 min	1500	126	WC, 40–70 nm	100	305
SPS [127]	1400 °C/2 min	180	50	WC–0.3 wt% VC–0.5 wt% Cr_3C_2, 200 nm	97.5	240
SPS [63]	1600 °C/5 min	105	50	WC–3 wt% ZrC, 700 nm	100	
SPS [64]	1300 °C/5 min	600	30	WC–6 wt% ZrO_2, 200 nm	99.9	
PECS[g] [83]	1900 °C/1.5 min	200	60	WC, 200 nm	100	280
PECS [109]	1700 °C/1.5 min	200	60	WC–5 vol% ZrO_2, 200 nm	100	
PCAS[h] [100]	1450 °C/0 min	900	80	WC–10 vol% Al_2O_3, <0.5 µm	98	112
SPS [128]	1450 °C/0 min	100	30	WC–2.8 wt% Al_2O_3–6.8 wt% ZrO_2, 0.8 µm	99	
HFIHS[i] [129]	1500 °C/100 s	1400	60	WC, 400 nm	98.5	380
HFIHS [130]	1250 °C/0 min	N/A	80	WC, 40 nm	99	87

[a]Hot pressing; [b]Hot isostatic pressing; [c]HIgh pressure and high temperature; [d]Gas protection sintering; [e]Spark plasma sintering; [f]Reactive spark plasma sintering; [g]Pulsed electric current sintering; [h]Pulsed current activated sintering; [i]High frequency induction-heated sintering

and (iv) thermal residual stress field resulting from mismatch in coefficients of thermal expansion of ceramic matrix and particulates as well as (v) the grain size [132, 133].

With respect to BTC, the most used dispersed phases are Al_2O_3 [95, 99], MgO [134–137], TiC [79], SiC [71, 87, 90], Mo_2C [85], and ZrC [63]. Qu et al. [101] successfully prepared WC–Al_2O_3 composite by employing conventional hot-pressing sintering. Al_2O_3 grains were homogenously distributed in WC matrix as demonstrated in Fig. 9. Excellent fracture toughness of 10.43 MPa m$^{1/2}$ was obtained for WC–40 vol% Al_2O_3 composite. It is noted from Table 5 that significant toughening effect was achieved due to the dispersed Al_2O_3 particle. Figure 9e–h illustrates the Vickers indentation crack extension path of WC–Al_2O_3 composites. With the increasing Al_2O_3 content, the crack propagation path became more tortuous, and more crack bridgings and crack deflections were observed. Additionally, WC–40 vol% Al_2O_3 composites exhibited secondary crack pattern as

depicted in Fig. 9h. The generation and existence of secondary crack consumed the energy of main crack and increased the length of crack propagation path, resulting in improved fracture toughness.

Recently, we prepared nano-laminated WC–Al_2O_3–TiC ceramics with a high fracture toughness of 11.49 MPa m$^{1/2}$ [138, 139]. Al_2O_3 crack deflection, transgranular Al_2O_3, microcracking, WC crack bridging, and plate-like WC crack deflection were the major toughening mechanisms (Fig. 10). Resulting from the thermal expansion mismatch between the secondary phase and the matrix, the residual stresses acting on WC/Al_2O_3 interfaces played a crucial role in the enhancement of grain boundary strength and then significantly improved the toughness of the matrix. As shown in Fig. 11, nanosized Al_2O_3 grains were located at the interface of WC grains and formed inter-granular structure, which hindered the WC grain growth and changed the grain shape. Nano-grained TiC grains were found to be embedded either
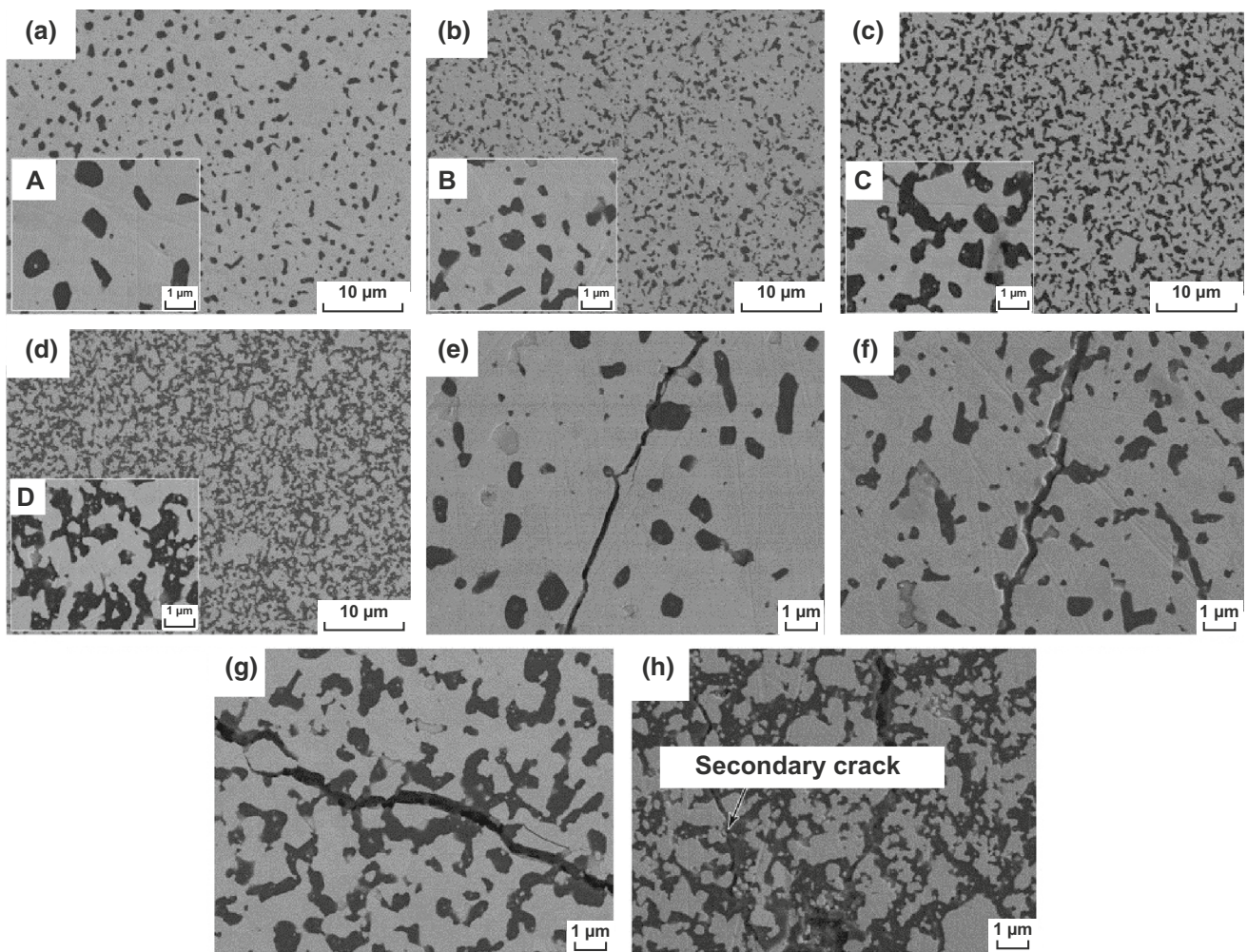
Fig. 9 FE-SEM images of the polished samples showing the different dispersion states and morphologies of the toughening particulates: (**a, A**) WC–10 vol% Al$_2$O$_3$, (**b, B**) WC–20 vol% Al$_2$O$_3$, (**c, C**) WC–30 vol% Al$_2$O$_3$, and (**d, D**) WC–40 vol% Al$_2$O$_3$, composites sintered at 1540 °C for 90 min. FE-SEM images of Vickers indentation crack extension path of **e** WC–10 vol% Al$_2$O$_3$, **f** WC–20 vol% Al$_2$O$_3$, **g** WC–30 vol% Al$_2$O$_3$, and **h** WC–40 vol% Al$_2$O$_3$ composites sintered at 1540 °C for 90 min [101]. Figure panels reproduced from Ref. [101] with permission from Elsevier copyright 2012

Table 5 Composition proportion, relative density and fracture toughness of WC–Al$_2$O$_3$ composites [101]

WC (vol%)	Al$_2$O$_3$ (vol%)	Sintering process	Relative density (%)	Fracture toughness K$_{IC}$ (MPa m$^{1/2}$)
90	10	1540 °C	95.73	7.86
80	20	90 min	96.52	8.10
70	30	39.6 MPa	96.53	9.43
60	40		97.98	10.43

in the WC matrix or at the WC grain boundaries, forming either intra-granular or inter-granular structure. Microcracks were found to be segregated inside alumina crystals (Fig. 11a). This might be a pinning effect caused by alumina grains and would substantially increase the number of potential sources of crack branching. Furthermore, dislocation

morphologies were found to exist both at the WC/Al$_2$O$_3$ interfaces (Fig. 11b) and inside alumina crystals (Fig. 11c, d), which could increase the flaw tolerance of the material and enhance the toughness of the material.

3.2 Transformation Toughening

Transformation toughening has been proved to be a significant approach to improve the toughness of ceramics [140–142]. Transformation toughening takes place, resulting from a stress-induced phase transformation of particulate inclusions in a ceramic matrix during fracture process, in which the most used particle is ZrO$_2$ partially stabilized with Y$_2$O$_3$ or MgO. It depends on the transformation of metastable retained tetragonal zirconia to the stable monoclinic zirconia phase in the tensile stress field around a crack tip. Compressive stresses are introduced in the matrix due to shear deformation (1–7%) coupled with volume expansion (4–5%) resulting from monoclinic phase occupying more volume in comparison with tetragonal phase. The compresses, acting as closure stresses, reduce the local crack tip stress intensity, thereby enhancing the toughness of the matrix [143].

Significant toughness improvement was obtained for WC–ZrO$_2$ composite by incorporating ZrO$_2$ particles into WC matrix [109–111]. Mukhopadhyay et al. [144] reported that WC–6 wt% ZrO$_2$ exhibited a toughness of 10.9 MPa m$^{1/2}$, which is only modestly lower by 16% in comparison with that of reference WC–6 wt% Co cemented carbide, while the flexure strength enhanced by 18%. By comparing the XRD patterns of polished and fractured surface of same specimen, the author [104] found the presence of a strong m-ZrO$_2$ peak with an intensity-reduced t-ZrO$_2$ peak in the fractured surface, identifying the transformation of $t \rightarrow m$-ZrO$_2$ during the fracture process, which was the principle source of toughening. Furthermore, the author proposed that the toughness of WC–ZrO$_2$ composite can be no more elevated with more than ∼6 wt% ZrO$_2$ addition. The presence of ZrO$_2$ grains in the WC matrix as a discrete second phase enables the former to behave in an intrinsic manner, that is, to undergo the $t–m$ transformation or to be retained as the metastable tetragonal form
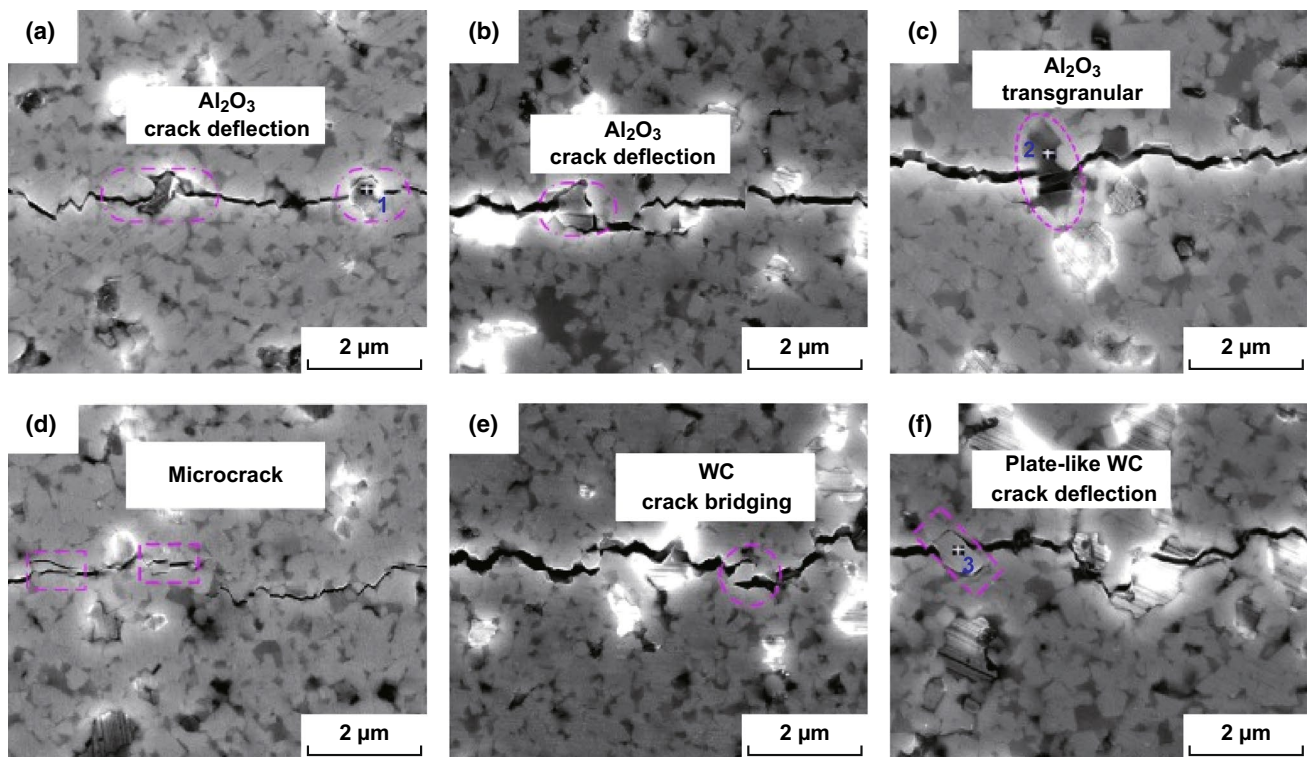
Fig. 10 Toughening mechanisms in WC–Al$_2$O$_3$–TiC ceramics: **a, b** Al$_2$O$_3$ crack deflection, **c** Al$_2$O$_3$ transgranular, **d** microcracking, **e** WC crack bridging and **f** plate-like WC crack deflection [138]. Figure panels reproduced from Ref. [138] Elsevier copyright 2018
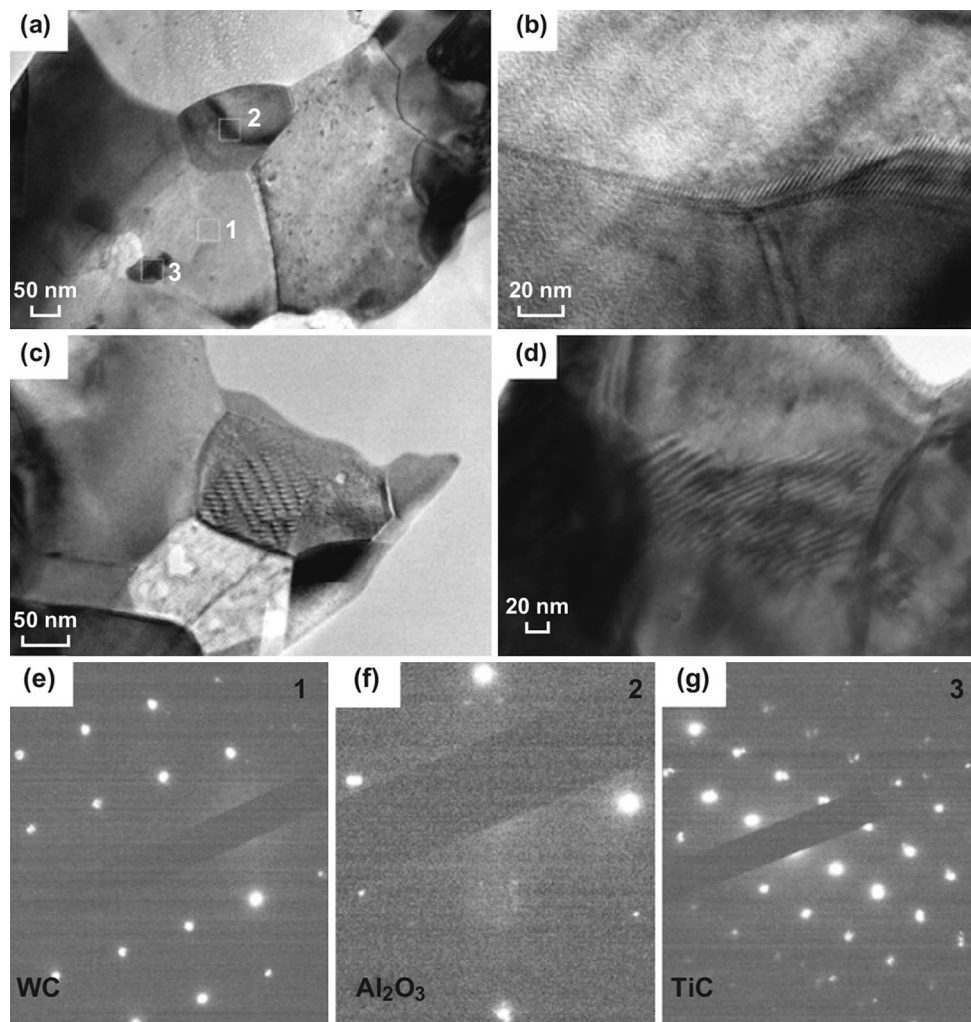
Fig. 11 a TEM micrographs of WC–TiC–Al$_2$O$_3$ ceramics, **b-d** dislocation morphology, and electron diffraction spots of **e** point 1, **f** point 2, and **g** point 3 [138]. Figure panels reproduced from Ref. [138] with permission from Elsevier copyright 2018

during cooling from the sintering temperatures. Thermally induced monoclinic transformation during the cooling process would result in the formation of microcracks around the transformed monoclinic ZrO$_2$ particles. The microcracks are effective to toughen the materials by absorbing fracture energy, but the linkup or coalescence of the microcracks, as a result of added ZrO$_2$ increasing, can reduce the toughness significantly. Therefore, it can be concluded that the highest toughness for WC–ZrO$_2$ composite can be achieved by adding about ~6 wt% ZrO$_2$ containing both tetragonal and monoclinic particles.

Wang [145] demonstrated that there existed a critical grain size for tetragonal ZrO$_2$ retention during cooling from the sintering temperature to a given temperature, above which the tetragonal ZrO$_2$ would transform to the monoclinic phase

during the cooling process. In other words, the fraction of retained t-ZrO$_2$ decreases with the increasing ZrO$_2$ particle size. Therefore, a grain growth inhibitor addition is beneficial for the transformation toughening. Zheng et al. [146] reported that the toughness of WC–8 wt% ZrO$_2$ was insensitive to the coarseness of microstructure and enhanced to 11 MPa m$^{1/2}$ as a function of VC together with Cr$_3$C$_2$ addition.

3.3 Whiskers Toughening

Profound toughening has been achieved in numbers of ceramics by incorporating whiskers. Compared with other toughening methods such as ZrO$_2$ transformation toughening, whisker toughening enjoys a potential advantage that

is the retention of high-toughness values at temperatures exceeding 1000 °C. Though sharing the similar toughness level with continuous-fiber-reinforced ceramics, whisker-reinforced composites possess advantages of easier fabrication as well as a higher degree of isotropy in mechanical properties because of the smaller aspect ratios involved. It is reported that five toughening mechanisms may be operative in whisker-toughened ceramics, that is, crack deflection, crack bowing, microcracking, whisker pullout, and crack bridging [147–149].

Though the number of researches and publications in whisker-toughened ceramics increased significantly, there are only a few reports with respect to BTC toughened by whiskers. Silicon carbide whiskers (SiC_w), as a reinforcing agent, exhibited a prominent effect on improving the toughness of ceramics [150]. Chao et al. [151] suggested that it was feasible to toughen WC ceramics by using SiC_w instead of metallic binder phase. The toughness of WC–SiC_w was increased by 30-40% in comparison with pure WC, due to SiC_w addition. Sugiyama et al. [88, 152] reported that a highly tough WC–3 vol% SiC_w composites with an initial powder size of 0.71 μm, which were fabricated by SPS, had an improved fracture toughness about 7.8 MPa m$^{1/2}$ in comparison with pure WC (about 5.9 MPa m$^{1/2}$). The best toughening effect was achieved at 3–5 vol% SiC_w addition. Above 10 vol%, the toughness decreased from the maximums; however, it still maintained high levels above 7 MPa m$^{1/2}$. Additionally, the author demonstrated that proper sintering parameter was of great importance to achieve the best toughening effect for the reason that an excessively high sintering temperature would made SiC_w thick, coarsen, and balloon and thus lowered the aspect ratio of the whiskers. Furthermore, Bengisu et al. [147] proposed that the amount of toughening would decrease significantly if the surface oxygen content of SiC_w was high. A possible solution to this problem is to eliminate the oxide formation on SiC_w surface by acid leaching cleaning the whiskers or coating the whiskers with an oxidation-resistant material.

Besides SiC whisker, Si_3N_4 whisker is another most common ceramic whisker used as a toughening agent for ceramics. Zheng et al. [153–155] investigated the effect of in situ growing β-Si_3N_4 whiskers on toughening WC ceramics prepared by SPS. The formation of β-Si_3N_4 whiskers significantly improved the toughness to 10.94 MPa m$^{1/2}$ for

WC–Si_3N_4 sample from 6.69 MPa m$^{1/2}$ for pure WC. The major toughening mechanisms were found to be Si_3N_{4w} pullout and crack bridging by Si_3N_4 whiskers as shown in Fig. 12. Furthermore, the author found that at temperature above 1700 °C, β-Si_3N_4 grains ripened rapidly and grew into β-Si_3N_4 whiskers speedily; at 1450–1600 °C, WC grains grew slowly, while the growth of β-Si_3N_4 grain and the formation of β-Si_3N_4 whiskers were slow. Exploiting the kinetics difference between β-Si_3N_4 grain growth and WC grain growth, the author proposed a two-step sintering method. For sample heated to 1700 °C and then immediately cooled to 1600 °C with a holding time of 30 min, a plenty of Si_3N_4 whiskers formed and WC grains did not grow rapidly.

From an oxidation resistance point of view, Al_2O_3 whisker seems to be a more reasonable choice. Dong et al. [94] successfully fabricated WC–Al_2O_3 whiskers composites employing hot-pressing sintering as the assistance of VC as grain growth inhibitor. Maximum toughness (13.8 MPa m$^{1/2}$) was obtained for WC–10 wt% Al_2O_{3w} composites. The toughening mechanisms were crack bridging, crack deflection as well as ligamentary bridging between crack surfaces. When the whisker content was above 10 wt%, the toughness decreased with the increasing whiskers content. Generally speaking, whisker addition deteriorates the densification process, due to whiskers resisting particle rearrangement, resulting from extensive sliding distances along whisker boundaries during sintering as well as at high whisker aspect ratios, or ratios above a critical volume fraction [147]. Therefore, there are two opposing factors operating in whisker-reinforced composites, and those are toughening effect and densification deteriorating influence. Densification becomes more difficult with the increasing whisker content, resulting from the formation of a rigid network as a result of whiskers coming into contact with each other. As the whiskers further increased beyond a critical value, for example 10 wt% in Dong's research [94], the densification deteriorating influence started dominating and then the toughness was decreased.

3.4 Laminated Structures and Functional Gradient Materials (FGM)

Besides optimizing the chemical composition, another strategy to enhance the fracture toughness of ceramics is through the design of ceramic laminates. Residual
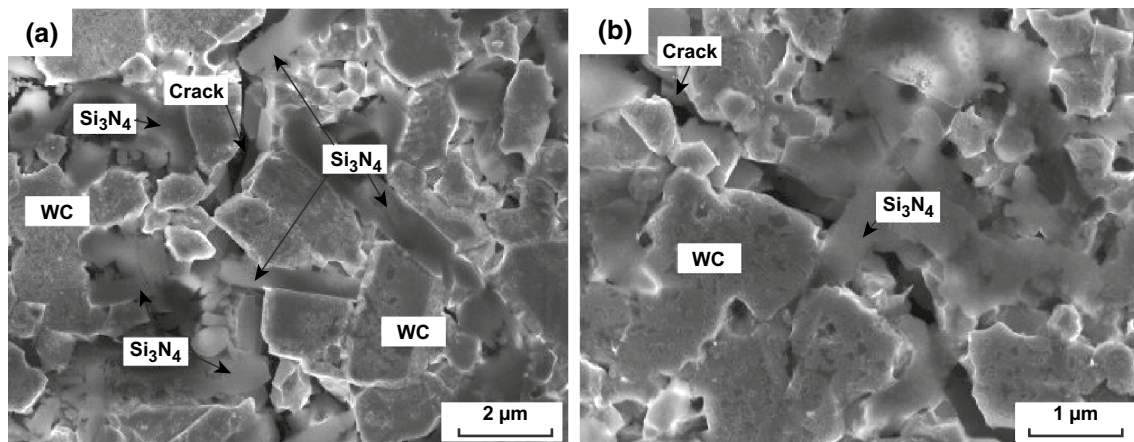
Fig. 12 SEM images of indentation cracks observed in the sintered WC–Si_3N_4 composites: **a** Si_3N_4 whiskers pullout, **b** crack-bridging by Si_3N_4 whiskers [153]. Figure panels reproduced from Ref. [153] with permission from Elsevier copyright 2013

stresses are inevitably set up during the cooling of layered ceramics, due to the mismatch in thermal expansion coefficients as well as elastic moduli. Lakshminarayanan et al. [156] demonstrated that a residual compression stress of about 400 MPa developed in the surface layer of a three-layered Al_2O_3–ZrO_2 ceramics significantly enhanced the fracture toughness to 30 MPa $m^{1/2}$ where the intrinsic fracture toughness was only 5–7 MPa $m^{1/2}$. Blugan et al. [157, 158] reported that apparent fracture toughness of 18 MPa $m^{1/2}$ was obtained for micro-laminated Si_3N_4–TiN composites, as a result of the formation of surface compressive stresses. It can be concluded that the residual stresses can be tailored to obtain high surface compressive stress, resulting in the great enhancement of fracture toughness.

Recently, we successfully prepared nano-laminated WC–Al_2O_3–TiC composites with the assistance of Cr_3C_2 and VC as grain growth inhibitor (Fig. 13) [139]. Because the coefficient of thermal expansion of TiC (7.74×10^{-6}/°C) and Al_2O_3 (8.8×10^{-6}/°C) is higher than that of WC (3.84×10^{-6}/°C), an increase content of TiC and Al_2O_3 from surface layer to core layer and a decrease content of WC from surface layer to core layer contributed to the generation of significant residual compressive stress on the surface of material, leading to the significant toughness enhancement.

3.5 New-Concept Toughening (Carbon Nanotube and Graphene Toughening)

Carbon nanotube (CNT), a one-dimensional (1D) nanomaterial discovered by Iijima [159] in 1991, has captured tremendous interests among scientific community and industry, owing to its high aspect ratio together with extraordinary mechanical, electronic, thermal, magnetic, and optical characteristics [160]. Many of these exceptional properties can be effectively exploited through incorporating carbon nanotube into BTC matrix, aiming to significantly improve the mechanical properties, fracture behavior, and functional features.

Shon et al. [161] reported the production of highly dense WC–CNT composites employing HFIHS under a pressure of 80 MPa within 3 min. The fracture toughness of obtained WC, WC–5 vol% CNT, and WC–10 vol% CNT was 7, 10.5, and 11 MPa $m^{1/2}$, suggesting that CNT addition significantly enhanced the toughness of BTC. The primary toughening mechanism was crack deflection by CNT as shown in Fig. 14a, b. Furthermore, the author demonstrated that the CNT addition was beneficial for the densification of WC. Bai et al. [162–164] demonstrated that adding CNT into WC-based matrix significantly enhanced the toughness, resulting from crack bridging, CNTs debonding, crack deflection, and CNT pullout. Jang et al. [165] reported that 46.8% increment
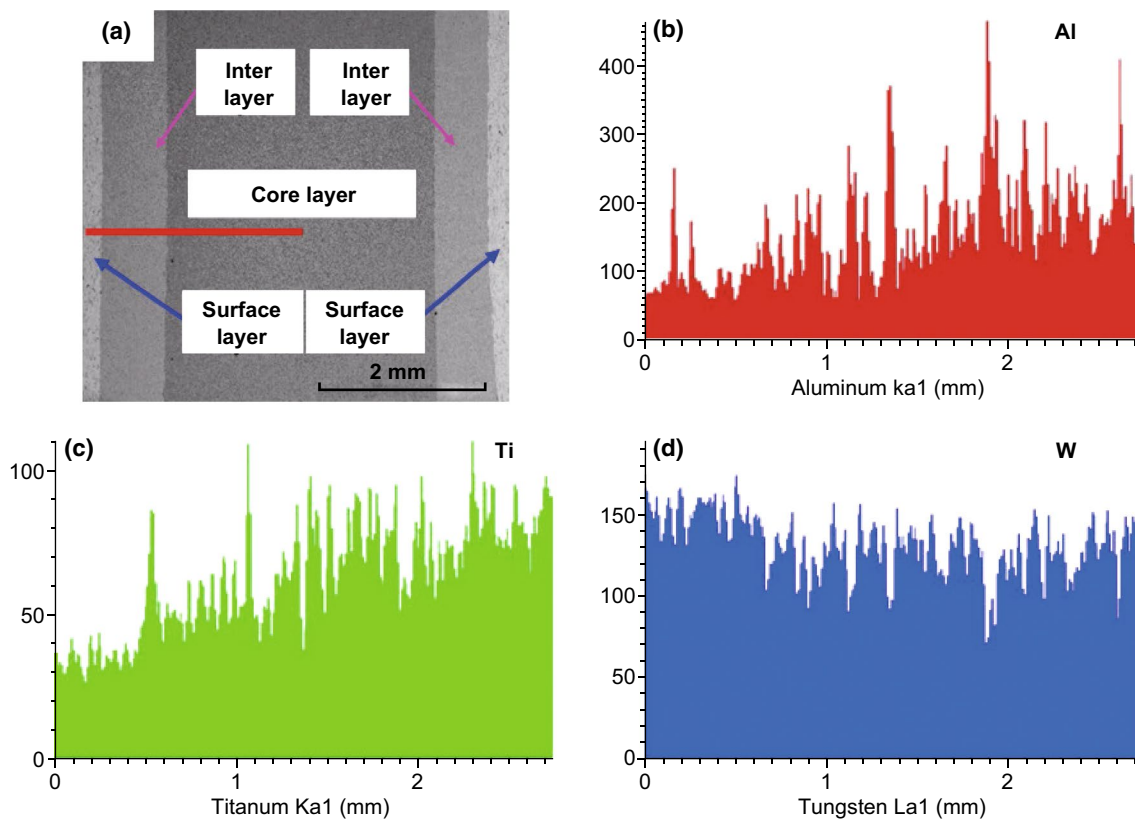
Fig. 13 a SEM micrographs and EDS maps of the distribution of **b** Al **c** Ti, and **d** W elements on the red line of nano-laminated WC–Al$_2$O$_3$–TiC ceramics [139]. Figure panels reproduced from Ref. [139] with permission from Elsevier copyright 2017. (Color figure online)

in fracture toughness was obtained for WC as a function of 15 vol% CNT addition, demonstrating that CNT prevented crack propagation by shielding a stress field in front of the crack tip or by bridging the crack forming ligaments behind the crack tip. Cao et al. [166] prepared ultra-fine-grained WC–1.0 wt% CNT composites with a high toughness of 9.11 MPa m$^{1/2}$ using SPS and investigated the effect of sintering temperature on the structure of CNT. In addition to crack deflection by CNT, CNT pullout was identified as another toughening mechanism as illustrated in Fig. 14c, d. Moreover, the author found that the structure of CNT was destroyed and CNT transformed to graphite phase in 1900 °C, indicating that WC–CNT composites should be sintered at moderate temperatures.

Besides CNT, graphene is another nanocarbon material, but possesses a unique two-dimensional (2D) sp^2 structure with considerable theoretical specific surface area (~ 2630 m^2 g^{-1}) and distinctive mechanical properties (e.g., breaking strength 42 N m^{-1}, tensile strength 130 GPa, stiffness 300–400 N m^{-1}, thermal conductivity 3000–5000 W m^{-1} K^{-1}, spring constant 1–5 N m^{-1}, and Young's modulus 0.5–1 TPa) [167, 168]. The 2D structure endows graphene with inherent advantages over other carbon allotropes as CNT. Furthermore, graphene possesses better dispersion properties than CNT and can be homogeneously dispersed into a ceramic matrix, which is another rather advantageous factor in improving the microstructure and mechanical properties of the ceramic composites [169, 170]. Additionally, graphene is endowed with energy dissipating mechanism by generating graphene bending and kinking. The coordination deformation of graphene consumes strain energy and then reduces the crack extension energy, significantly contributing to the improvement of fracture toughness [171]. All these properties are very attractive for the application of graphene as reinforcement for ceramic composites [172].

It is reported that graphene showed remarkable effectiveness in enhancing the fracture toughness of Al$_2$O$_3$-based ceramics [173], Si$_3$N$_4$-based ceramics [174], ZrB$_2$-based ceramics [175], ZrO$_2$-based ceramics [176], and TaC-based
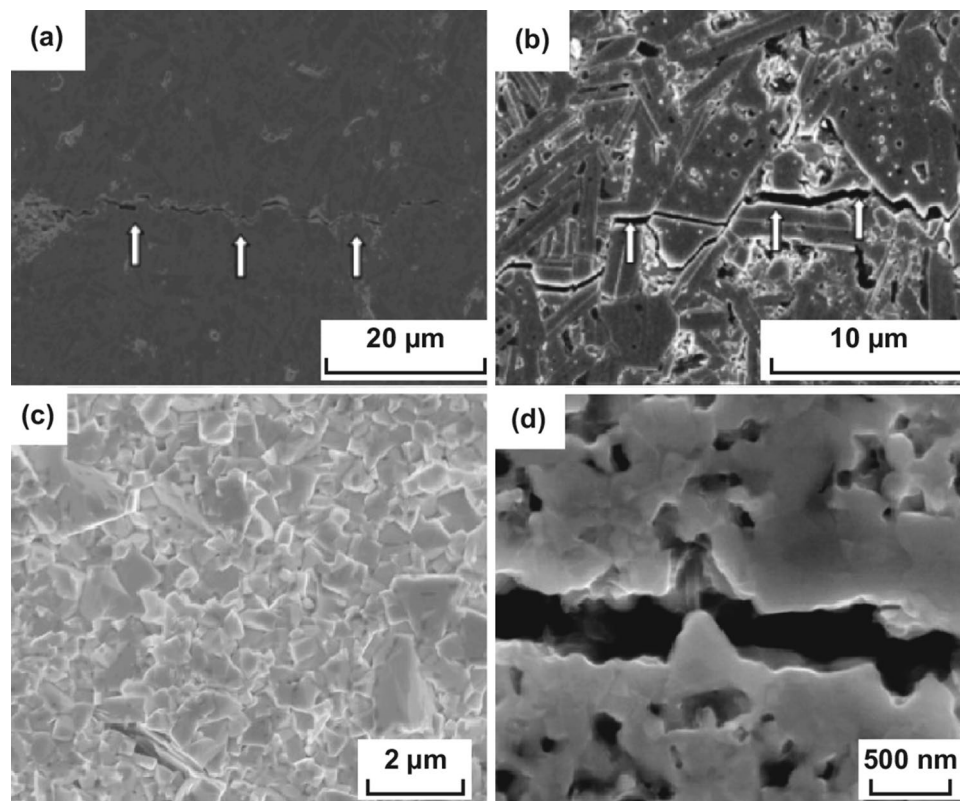
Fig. 14 FE-SEM micrographs of crack propagation in **a** WC–5 vol% CNT and **b** WC–10 vol% CNT [161]. Typical SEM images of **c** the fracture surfaces and **d** crack details of WC–CNT composites [166]. Figure panels reproduced from Ref. [161] with permission from INST Problems Mechanical Engineering-Russian Card Sciences copyright 2011, Ref. [166] with permission from Elsevier copyright 2018

ceramics [177]. To the best of our knowledge, few studies have been reported on the effects of graphene addition on the densification and properties of BTC materials hitherto.

Recently, we investigated the toughening effect of multilayer graphene (MLG) on BTC through hot-pressing method [178]. It is worthwhile mentioning that the achievement of good graphene/WC composites depends extremely on three critical factors, and those are homogeneous dispersion within the WC matrix, minimization of the mechanical damage of graphene, and optimum bonding between WC matrix and graphene. MLG was homogeneously dispersed in the WC-based ceramic matrix as shown in Fig. 15a. Figure 15b depicts Raman spectroscopy of MLG and sintered ceramics, implying the survival of MLG after the so-designed two-step sintering. Both the spectra presented the characteristic D, G, and 2D bands corresponding to MLG at ~ 1350, ~ 1580, and ~ 2700 cm^{-1}, confirming that the graphene-based structure has not been damaged during the milling and sintering processes. WC-based ceramics with 0.1 wt% MLG addition

exhibited a fracture toughness of 14.1 MPa m$^{1/2}$, undergoing ~ 53.3% enhancement in comparison with monolithic ceramics. MLG bending, wrapping, interface debonding, MLG wall and network, MLG-induced weak interface, grains bridging by MLG, MLG pullout, crack deflection, crack bridging, and crack stopping were the major toughening mechanisms (Fig. 16). Also, the preferential orientation of MLG in WC matrix and MLG intrinsic energy dissipating mechanisms as sheet kinking, bending, and sliding played very significant roles in contributing to the toughness enhancement of BTC reinforced by MLG. The detailed discussion about the toughening mechanism in WC/MLG composites can be found in our previous article [178].

3.6 Synergistic Toughening

An area of remarkable potential is the synergistic toughening, taking advantage of the possibilities of multiple toughening mechanisms operative within a single composite. It is
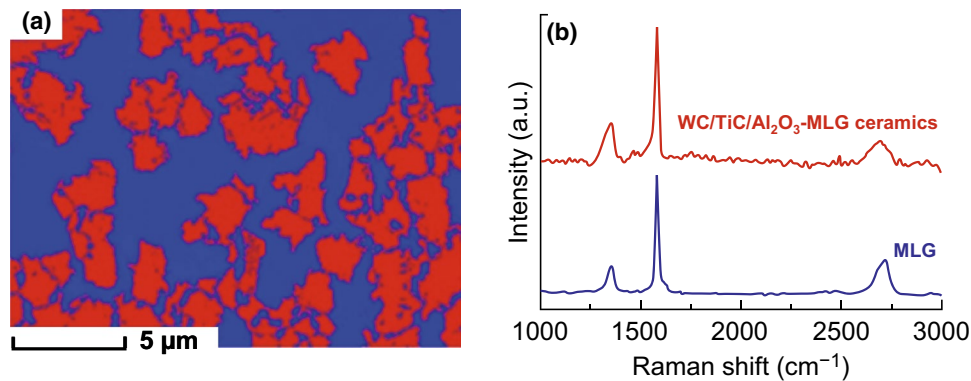
Fig. 15 a The distribution of MLG (color in red) in WC-based composites reinforced by 0.1 wt% MLG (by EBSD). **b** Raman spectroscopy of MLG and sintered ceramics [178]. Figure panels reproduced from Ref. [178] with permission from Elsevier copyright 2017. (Color figure online)

suggested from both theoretical analysis and experimental observations that the overall effect of combined toughening mechanisms may be greater than the sum of the increments from individual components.

Combining secondary-phase reinforcements, such as platelets as well as whiskers, with microstructural tailoring of the matrix may be of great potential. Also, transformation toughening could be combined with other toughening methods. Furthermore, toughening by designing laminated structure combined with toughening by the design of chemical composition would be of significant promise to improve the fracture toughness of ceramics. By combining particle dispersion toughening (with Al_2O_3) with transformation toughening (with ZrO_2), Xia et al. [128] prepared WC–Al_2O_3–ZrO_2 composites with high fracture toughness. Bai et al. [163] reported a highly tough WC–Al_2O_3–CNT composite coupling carbon nanotube toughening with Al_2O_3 particle dispersion toughening. Combining particle dispersion toughening, graphene toughening, and laminated structure toughening, we prepared highly tough laminated WC–Al_2O_3–TiC–MLG composite [178].

# 4 Mechanical Properties of Binderless Tungsten Carbide

Mechanical properties of BTC are strongly dependent on their densification degree, grain size, chemical compositions as well as microstructure. Hardness and fracture toughness, the critical properties in many applications of engineering structural materials, are the most important intrinsic mechanical properties for BTC. Despite its high hardness as well as excellent wear/corrosion/oxidation resistance, a major limitation of BTC's further applications, structural application as an example, is its poor fracture toughness. Enhancing the fracture toughness without sacrificing hardness is invariably one of the goals of BTC development. Wear resistance of BTC is also one of the most significant mechanical properties; however, it is mostly determined by the hardness coupled with fracture toughness.

4.1 Hardness Versus Fracture Toughness

Hardness is always a stress standing for the resistance to non-recoverable deformation of a material, while fracture toughness characterizes a material's resistance to crack propagation and, as such, is measured as the fracture energy. They are the two basic mechanical properties of BTC and the foundation of other mechanical properties, such as wear resistance, flexural strength as well as impact resistance.

The mechanical properties of pure WC were reported in several researches. Date demonstrates that the fracture toughness of pure WC decreased with the increasing hardness (Fig. 17a), which is similar to the general tendency of conventional WC–Co cemented carbide. It should be noted that for WC–Co cemented carbides, Co binder phase acts for impeding the crack propagation through shielding a stress in front of crack tip. However, in pure WC, crack propagates along the WC/WC interface or penetrates into large WC grains, implying that the large WC grains together with the remaining small pores prevent crack growth and absorb
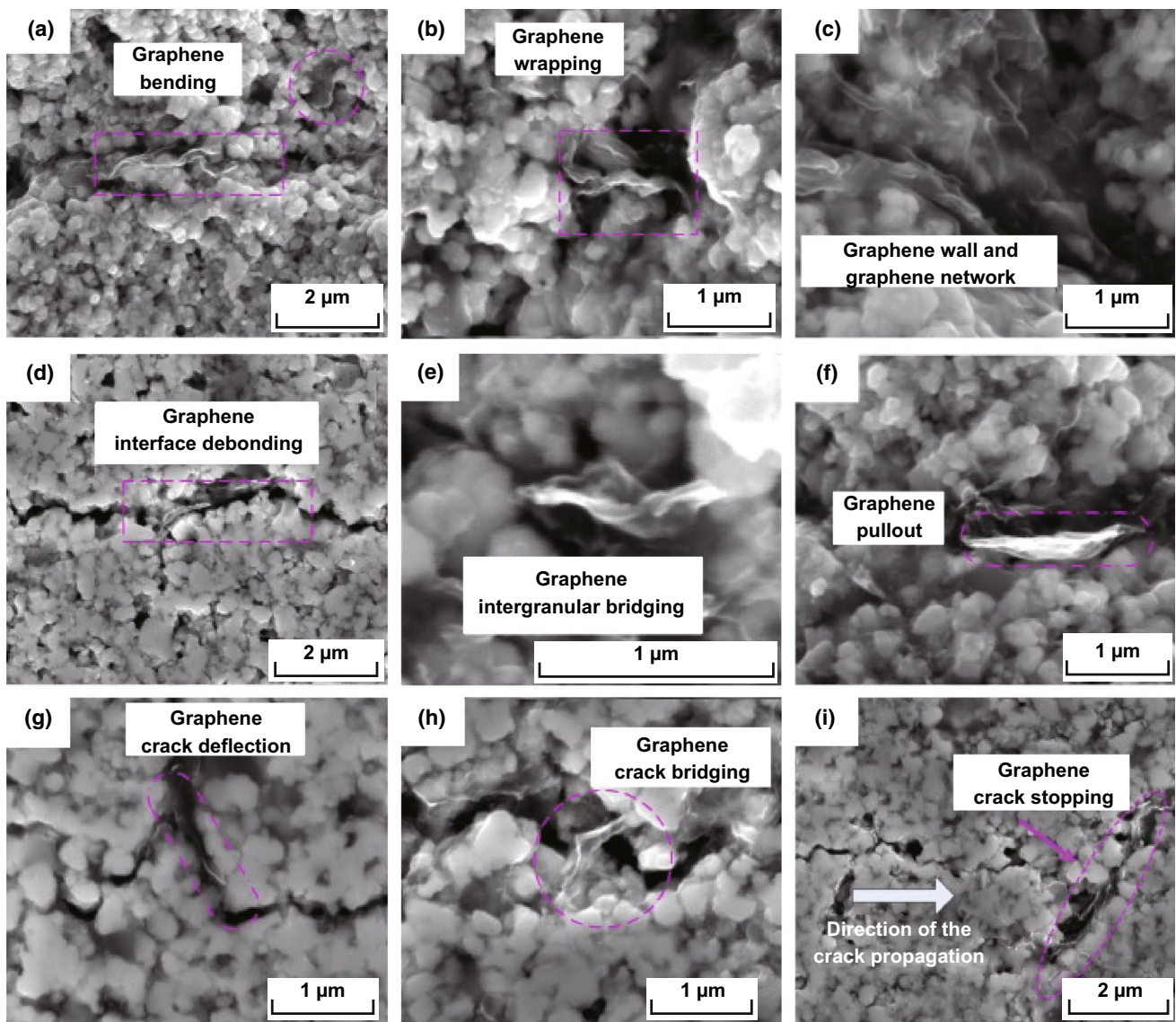
Fig. 16 Toughening mechanisms in WC-based ceramics reinforced by MLG: **a** graphene bending, **b** graphene wrapping, **c** graphene wall and network, **d** graphene interface debonding, **e** graphene intergranular bridging, **f** graphene pullout, **g** graphene deflection, **h** crack bridging, and **i** crack stopping [178]. Figure panels reproduced from Ref. [178] with permission from Elsevier copyright 2017

fracture energy. Furthermore, the mechanical properties of BTC can be remarkably enhanced by improving the densification. As shown in Fig. 17b, c, both hardness and fracture toughness were improved with the increase in the relative density, and high mechanical properties (hardness and fracture toughness) corresponded to high density. Also, it is revealed that Hall–Petch-like relationship is applied to BTC as shown in Fig. 17d, implying that hardness enhancement of BTC is associated primarily with obtaining fine grain in the sintered material at a given relative density.

It has been recognized that the reduction in microstructural scale to nanometer resulted in substantial enhancement in mechanical properties of BTC. The trade-off relationship between hardness and fracture toughness may be reduced when the grain sizes approach nanoscale as 100 nm. With respect to conventional BTC, the fracture toughness reduces with increasing hardness; however, the hardness increase in nanosized BTC does not lower or even increase the fracture toughness. Though possessing higher relative density (99.1%), micro-sized WC (400 nm) exhibited both lower
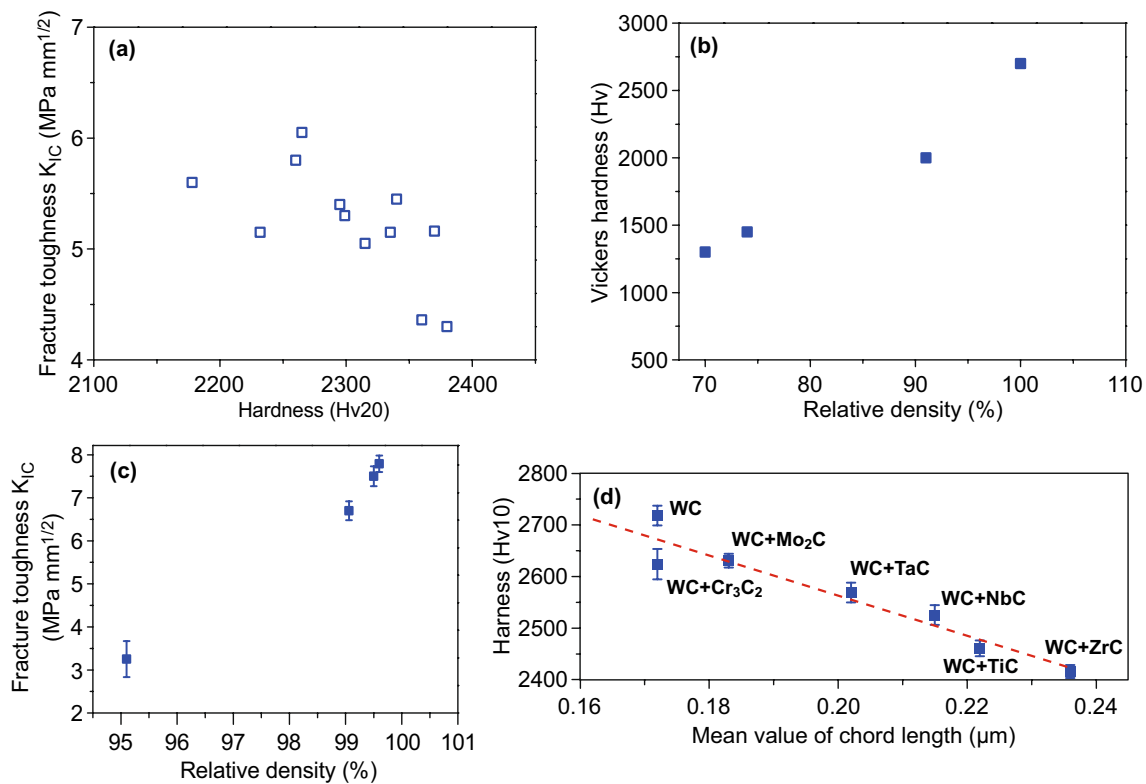
Fig. 17 **a** Plot of fracture toughness versus hardness of BTC [126]. **b** Plot of hardness and **c** fracture toughness versus relative density [119, 179]. **d** Plot of hardness versus chord length of dense samples [180]. Figure panels reproduced from Ref. [126] with permission from IEEE copyright 2005, Ref. [119] with permission from Elsevier copyright 2006, Ref. [179] with permission from Elsevier copyright 2017, Ref. [180] with permission from EPMA copyright 2014

hardness (27.5 GPa) and toughness (4.5 MPa m$^{1/2}$) in comparison with nanosized WC (87 nm) having a hardness of 29.6 GPa and toughness of 7.1 MPa m$^{1/2}$ [130, 181].

Table 6 illustrates hardness and fracture toughness of some reported BTC with various chemical compositions, relative densities, and grain sizes. As discussed before, some carbide addition can improve the sinterability of BTC; however, the carbide-added BTC, such as WC–TiC, WC–VC, and WC–TaC, exhibited a deteriorated hardness and similar or slightly lower fracture toughness in comparison with pure WC. Metal-oxide-added WC-based composites, such as WC–Al$_2$O$_3$, WC–MgO, and WC–ZrO$_2$, showed a good combined property similar to or even better than conventional WC–Co cemented carbide. Grain growth inhibitor is essential for WC-based composites to further improve mechanical properties, regardless of carbide addition or oxide addition. Graphene-reinforced WC-based composites exhibited the best combined property.

4.2 Wear Resistance

Liu et al. [187] studied the wear resistance of pure WC. The experiments were ball-on-disk type, in which ball is the SiC counterpart ball with a diameter of 6.25 mm and a hardness of 28 GPa, and disk is WC. The test temperature increased from 25 to 800 °C under air and vacuum conditions. The results showed that pure WC can maintain phase stability at the temperature till 800 °C in vacuum. In air, the wear mechanism of pure WC was mainly oxidation wear, and the critical temperatures causing degradation on the wear properties were 500 and 550 °C.

Engqvist et al. [188] compared the sliding wear resistance of WC–TiC–TaC with conventional WC–Co cemented carbides and ceramics as Al$_2$O$_3$ and SiC (Table 7). Three kinds of abrasive particles, including diamond, silicon carbide, and silica, were used. During the test, the normal load was 0.2 N and the total sliding distance was 50 m. The results showed

Table 6 Hardness and fracture toughness of some reported BTCs

Material	Relative density (%)	Sintered grain size (nm)	Hardness[a] (Hv)	Fracture toughness[b] (MPa m$^{1/2}$)
WC [18]	99.2	200	2925	8.9
WC [181]	100	130	3061	7.3
WC [182]	98.5	380	2854	7.1
WC [130]	99	87	3020	7.1
WC [125]	99.8	220	2959	7.2
WC [58]	97.6	360	2480	6.6
WC–20 at.% TiC [81]	98.5	200	2032	6.3
WC–20 at.% TiC [183]	99	200	2240	7.5
WC–3 wt% TiC–2 wt% TaC–0.2 wt% Cr$_3$C$_2$–0.2 wt% VC [184]		600	2300	7.9
WC–6 wt% Mo$_2$C [184]		250	2400	8.4
WC [84]	99.9	280	2795	4.38
WC–1 wt% VC [84]	96.5	280	2795	4.2
WC–1 wt% VC [185]	99.8	272	2585	6.9
WC–1 wt% Cr$_3$C$_2$ [185]	100	277	2605	7.2
WC–0.3 wt% VC–0.5 wt% Cr$_3$C$_2$ [119]	97.5	240	2875[d]	6.05
WC–0.33 wt% VC–0.54 wt% Cr$_3$C$_2$ [121]	97.9	730	2464	4.4
WC [180]	100.6	171	2720	7.0
WC–1 wt% Mo$_2$C [180]	100.8	183	2630	6.6
WC–1 wt% Mo$_2$C [85]	99	450	2461	4.8
WC–1 wt% TaC [180]	99.7	202	2570	6.9
WC–1 wt% ZrC [180]	98.8	236	2420	6.5
WC–1 wt% NbC [180]	99.6	214	2540	6.6
WC–6 mol% SiC–2 mol% ZrC [71]	99	720	2193[e]	6.7
WC–20 mol% SiC–0.3 mol% Cr$_3$C$_2$ [90]	99	420	2193	6.4
(WC–0.8 mol%Cr$_3$C$_2$)–5 vol% SiC$_w$ [152]	100.4	1500	2041	7
WC–14.3 wt% Al$_2$O$_3$–0.5 wt% VC [93]	98	2000	2103	11.54
WC–10 wt% Al$_2$O$_{3w}$–0.5 wt% VC [94]	98	2000	2103	13.8
WC–10 vol% Al$_2$O$_3$ [102]	99.8	101	2540	9.4
WC–4.3 wt% MgO [135]	99	2590	1878[f]	12.95
WC–6 wt% ZrO$_2$ [104]	100	660	1876	10.8
WC–3 wt% AlN [186]	99.6	700	2400	7.5
WC–10 wt% Si$_3$N$_{4w}$ [153]	100	1260	1801	10.94
WC–1.0 wt% CNT [166]	101	200	2328	8.95
WC–3 wt% Al$_2$O$_3$–2 wt% TiC–0.15 wt% MLG[c] [178]	98.9	400	2255	14.5

[a]For convenience of comparison, the original hardness values from papers were converted to Vickers hardness values

[b]Fracture toughness value was calculated from indentation method

[c]This is the surface layer of a functionally graded WC–AL$_2$O$_3$–TiC–MLG composites

[d]This is a value of HV0.5

[e]This is a value of HV1.0

[f]This is a value of HV30

that the WC–TiC–TaC had a slightly lower wear resistance than WC–Co cemented carbides, but much higher than that of common engineering ceramics Al$_2$O$_3$ and SiC as demonstrated in Fig. 18a. The BTC was worn by a preferential removal of TiC grains, leaving the TaC/NbC and WC grains unsupported, which contributed to an increased wear rate in comparison with WC–Co cemented carbides, implying that TiC was a weak constituent of the binderless carbide.

Therefore, it is denoted that BTC composites free of TiC may have a superior wear resistance to conventional WC–Co cemented carbides. Based on this idea, Botton et al. [184] investigated the wear resistance of WC–6 wt% Mo_2C and WC–6 wt% Co (Table 8) as shown in Fig. 18b. The results demonstrated that WC–Mo_2C exhibited better wear resistance than WC–Co cemented carbides. The wear mechanism of WC–Mo_2C was found to be ductile, which was different from that of WC–TiC–TaC suffering from grain pullout of TiC. It seems that the wear resistance of BTC strongly depends on the bonding between the carbide grains, and WC–Mo_2C provided a better bonding than WC–TiC–TaC.

Venkateswaran et al. [106, 107] investigated the wear resistance of WC–ZrO_2 composites using a fretting wear tester employing bearing steel as a counter body on WC–ZrO_2 under the ambient condition of temperature and humidity, demonstrating that the abrasion and tribochemical wear resulting in WO_3 formation were the predominant wear mechanisms for WC–ZrO_2 composites.

Recently, we investigated the sliding wear resistance of MLG-reinforced BTC [178]. The results showed that the ab plane of MLG exhibited a preferential orientation perpendicular to the direction of applied pressing as shown in Fig. 19a, b, playing a rather significant role in enhancing the tribological performance of MLG-reinforced materials. MLG-reinforced WC exhibited ~73.8% decrement in friction coefficient and ~82.65% improvement in wear resistance in surface perpendicular to the direction of applied pressing in comparison with monolithic ceramics as illustrated in Fig. 19c, d. It is noted from Fig. 19e–h that both the depth and the width of the wear track of WC ceramics containing 0.1 wt% MLG are smaller than those of monolithic ceramics. The dramatic improvement in tribological performance is attributed to the self-lubrication of MLG and easily formed friction layer in the contact interface as shown in Fig. 20. Furthermore, the unrivaled thermal conductivity of MLG and its rather significant effect in inhibiting the grain growth

Table 7 Composition, grain size, hardness, and fracture toughness of the tested materials [188]

Specimen	Composition (wt%)	Grain size (μm)	Hardness (HV0.5)	Fracture toughness K_{IC} (MPa m$^{1/2}$)
B1	94.5WC, 2Ta/NbC, 3TiC, < 0.5Co	1.3	1900	7.9
F6	94WC, 5.4Co, 0.6(Ta, Nb)C	1.0	1720	10.8
C6	94WC, 6Co	7.0	1220	15
SiC	SiC + some free C	3.0	2300	4.5
Al_2O_3	96.95Al_2O_3, 0.25MgO, 2.8ZrO_2	1.9	1820	5.4
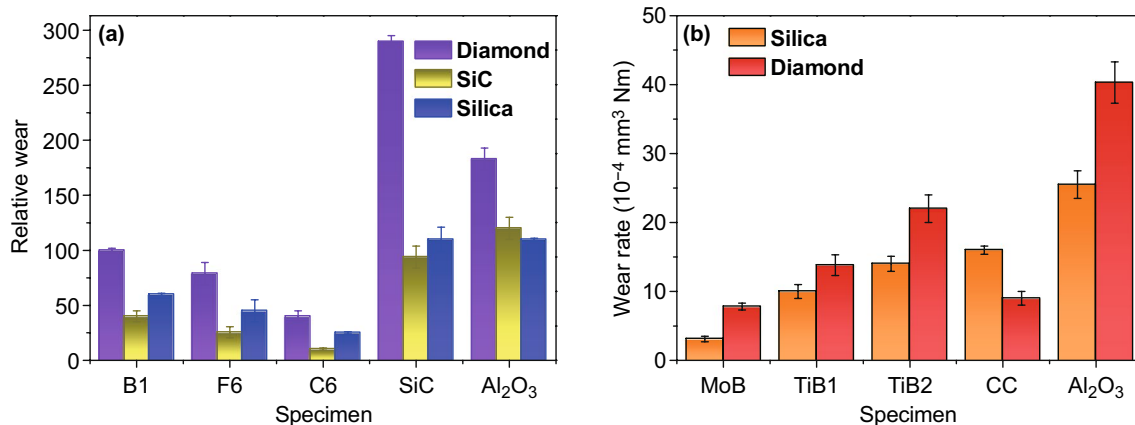
Fig. 18 **a** Relative wear rates for the tested materials as shown in Table 7 abraded with diamond, SiC, and silica. 100 corresponds to Bl worn with diamond [188]. **b** Wear rates for the different tested materials as shown in Table 8 abraded with silica and diamond [184]. Figure panels reproduced from Ref. [188] with permission from Springer Nature 1998, Ref. [184] with permission from Wiley copyright 2000

Table 8 Composition, grain size, hardness and fracture toughness of the tested materials

Specimen	Composition (wt%)	Grain size (μm)	Hardness (HV0.5)	Fracture toughness K_{IC} (MPa m$^{1/2}$)
MoB [184]	94WC, 6Mo$_2$O	0.25	2400	8.4
TiB1 [184]	94.6WC, 3TiC, 2TaC, 0.2Cr$_3$C$_2$, 0.2VC	0.6	2300	7.9
TiB2 [188]	95WC, 3TiC, 2TaC	2.0	1900	7.9
CC [188]	94WC, 6Co	7	1200	15
Al$_2$O$_3$ [188]	96.95Al$_2$O$_3$, 0.25MgO, 2.8ZrO$_2$	1.9	1820	5.4

are an important contribution to the improved tribological performance.

5 Concluding Remarks and Outlook

In this review, recent extensive investigations on the processing, microstructure, and mechanical properties of BTC and BTC composites are summarized. Such insights should be very helpful in tailoring the properties by judiciously selecting the chemical composition coupled with processing techniques and parameters.

Critical issue associated with the densification of BTC has been reviewed. It is believed that the densification of BTC is rather challenging due to the absence of metallic binder. The review highlights the crucial roles of mixed carbon content, carbide grain size, ceramic additive as well as advanced sintering techniques in the densification process. Carbon control is rather essential for BTC achieving maximum densification and performance levels. Strict design of additives including carbon, WO$_3$, and W together with carefully control of thermal processing process is of great importance to the carbon content in final product. Sintering temperature strongly depends on the grain size; thus, finer initial powder grain size is helpful in lowering the sintering temperature as well as shortening the sintering process, especially for nanopowders. Nanocrystalline WC powders possess better sinterability in comparison with micro-sized ones, due to their high surface energy increasing the sintering driving forces. Besides reducing the particle size of WC matrix, it is also effective to facilitate the sintering of WC by dispersing some nanosized second-phase additive within micro-sized WC matrix grains or at the grain boundaries of WC matrix. The low melting point of the metal and possibility of carbonation and oxidation make the selection of the transition-metal carbides (TiC, TaC, and SiC) and metal

oxides (Al$_2$O$_3$, ZrO$_2$, Y$_2$O$_3$, and La$_2$O$_3$) binders more favorable for consolidating WC powders. The advanced sintering techniques, such as SPS, RSPS, HFIHS as well as PCAS, are successfully employed in laboratory scale preparing dense BTC. Particularly, SPS is currently the most commonly used sintering method to consolidate BTC or BTC composites.

Another critical issue associated with the toughening of BTC has also been reviewed. Varieties of traditional toughening methods including particle dispersion toughening (Al$_2$O$_3$, MgO, etc.), transformation toughening (ZrO$_2$), whisker toughening (SiC$_w$, Si$_3$N$_{4w}$, Al$_2$O$_{3w}$), and synergistic toughening together with some new-concept toughening methods, such as laminated structure toughening, carbon nanotube toughening, and graphene toughening, have been proposed to toughening BTC. Particularly, new-concept toughening methods offered great promise of a revolutionary advance in the production of highly tough BTC. Furthermore, toughening by designing laminated structure combined with toughening by the design of chemical composition would be of significant promise to enhance the fracture toughness of BTC.

Mechanical properties of BTC are strongly dependent on their densification degree, grain size, chemical compositions as well as microstructure. The fracture toughness of pure WC decreases with the increasing hardness, which is similar to the general tendency of conventional WC–Co. Both hardness and fracture toughness can be improved with the increase in the relative density, and high mechanical properties (hardness and fracture toughness) correspond to high densification. The trade-off relationship between hardness and fracture toughness may be reduced when the grain sizes approach nanoscale as 100 nm. Compared with other materials reinforced BTC, graphene-reinforced BTC exhibited the best combined property. BTC has comparable or higher wear resistance than conventional WC–Co cemented carbides, but
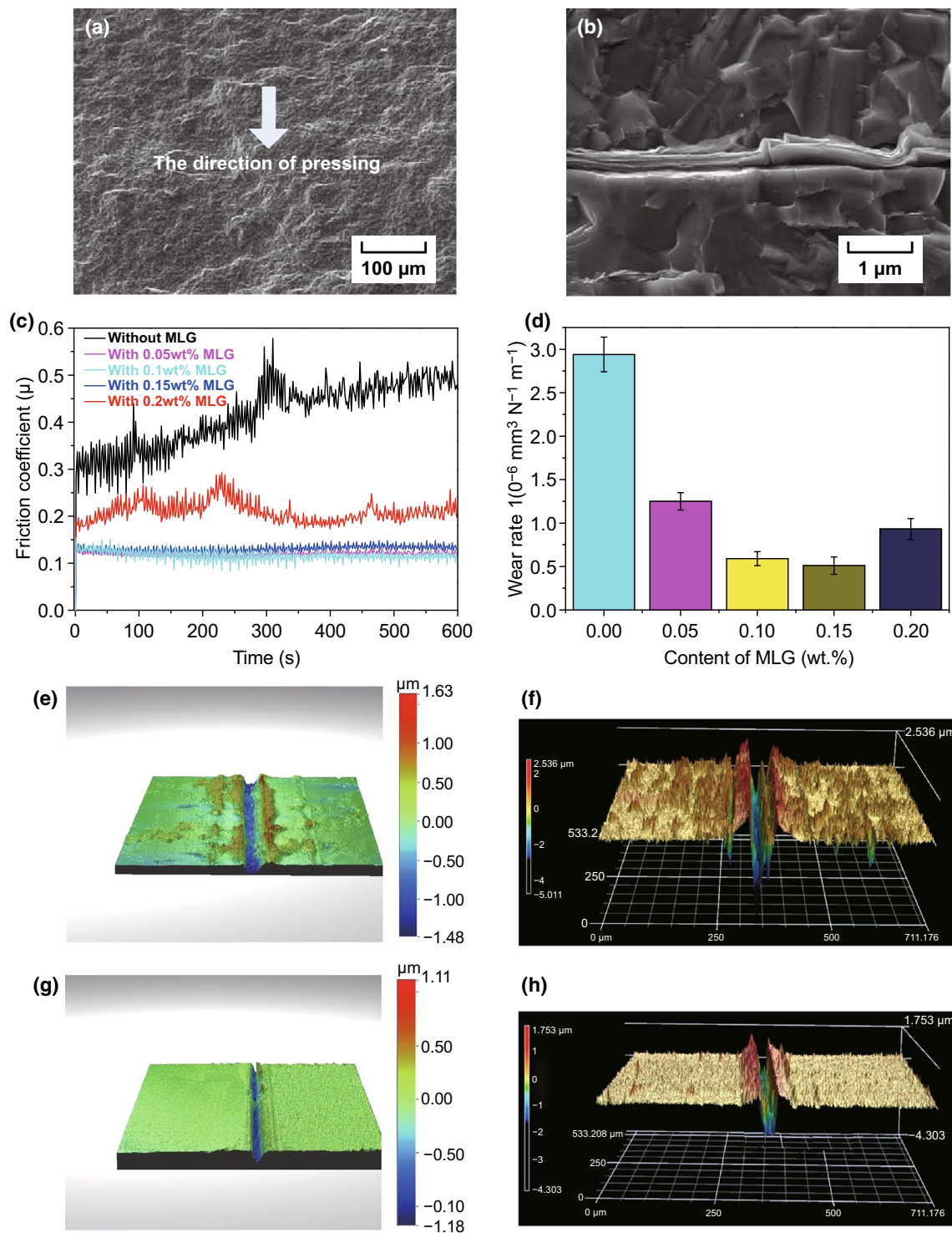
Fig. 19 Preferential orientation of MLG in WC ceramics after hot-pressing **a** in low magnification and **b** in high magnification, influence of MLG contents on **c** friction coefficient and **d** wear rates, surface topographies of wear tracks on **e**, **f** monolithic WC ceramics and **g**, **h** ceramics containing 0.1 wt% MLG [178]. Figure panels reproduced from Ref. [178] with permission from Elsevier copyright 2017
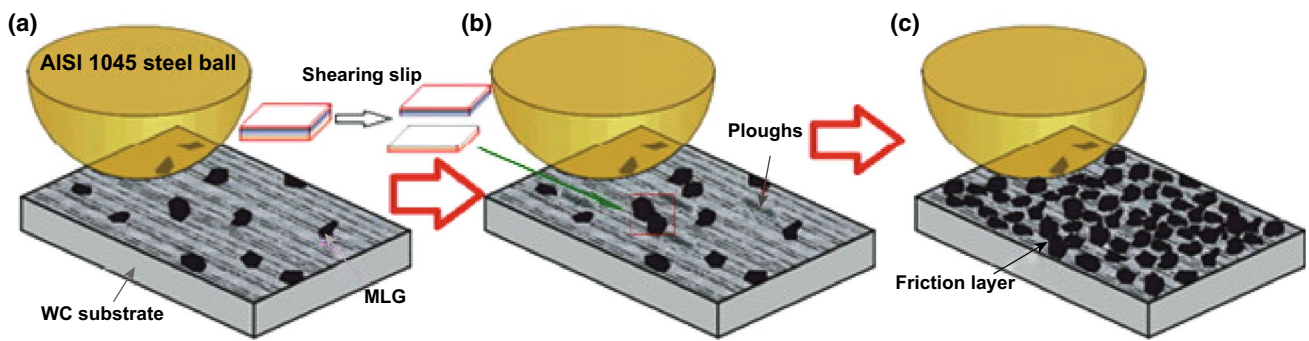
Fig. 20 Schematic of effect mechanism of MLG reinforced WC-based materials against AISI 1045 steel [178]. Figure panels reproduced from Ref. [178] with permission from Elsevier copyright 2017

much higher than that of common engineering ceramics such as Al_2O_3 and SiC.

Finally, it should be noted that, in spite of the progress made in the processing as well as properties of BTC, this remains a field of prospect, and further research is required to optimize chemical composition, further enhance mechanical properties as well as reduce manufacturing costs, develop sintering techniques for large scale production, develop new techniques as selective laser sintering for fabricating complex-shaped functional BTC composite powder parts, and advance them more widely and novel applications, so as to produce BTC or BTC composites on an industrial or commercial scale.

References

1. Z.Z. Fang, M.C. Koopman, H.T. Wang, Cemented tungsten carbide hardmetal—an introduction, in *Comprehensive Hard Materials*, ed. by D. Mari, L. Llanes, V.K. Sarin (Elsevier, Oxford, 2014), pp. 123–138. https://doi.org/10.1016/B978-0-08-096527-7.00004-0

2. L. Prakash, Introduction to hardmetals—fundamentals and general applications of hardmetals, in *Comprehensive Hard Materials*, ed. by D. Mari, L. Llanes, V.K. Sarin (Elsevier, Oxford, 2014), pp. 29–90. https://doi.org/10.1016/B978-0-08-096527-7.00002-7

3. R. Viswanadham, *Science of Hard Materials* (Springer, Berlin, 1983). https://doi.org/10.1007/978-1-4684-4319-6

4. A.V. Shatov, S.S. Ponomarev, S.A. Firstov, Hardness and deformation of hardmetals at room temperature, in *Comprehensive Hard Materials*, ed. by D. Mari, L. Llanes, V.K. Sarin (Elsevier, Oxford, 2014), pp. 647–699. https://doi.org/10.1016/B978-0-08-096527-7.00009-X

5. A.V. Shatov, S.S. Ponomarev, S.A. Firstov, Fracture and strength of hardmetals at room temperature, in *Comprehensive Hard Materials*, ed. by D. Mari, L. Llanes, V.K. Sarin (Elsevier, Oxford, 2014), pp. 301–343. https://doi.org/10.1016/B978-0-08-096527-7.00010-6

6. J.L. Sun, J. Zhao, F. Gong, X.Y. Ni, Z.L. Li, Development and application of WC-based alloys bonded with alternative binder phase. Crit. Rev. Solid. State. **44**(3), 211–238 (2019). https://doi.org/10.1080/10408436.2018.1483320

7. A. Mukhopadhyay, B. Basu, Recent developments on WC-based bulk composites. J. Mater. Sci. **46**(3), 571–589 (2011). https://doi.org/10.1007/s10853-010-5046-7

8. A. Krawitz, E. Drake, Residual stresses in cemented carbides—an overview. Int. J. Refract. Met. Hard Mater. **49**, 27–35 (2015). https://doi.org/10.1016/j.ijrmhm.2014.07.018

9. A.D. Krawitz, E.F. Drake, Residual stresses, in *Comprehensive Hard Materials*, ed. by D. Mari, L. Llanes, V.K. Sarin (Elsevier, Oxford, 2014), pp. 385–404. https://doi.org/10.1016/B978-0-08-096527-7.00013-1

10. D. Mari, A.D. Krawitz, J.W. Richardson, W. Benoit, Residual stress in WC–Co measured by neutron diffraction. Mater. Sci. Eng., A **209**(1–2), 197–205 (1996). https://doi.org/10.1016/0921-5093(95)10147-0

11. H.U. Sverdrup, K.V. Ragnarsdottir, D. Koca, Integrated modelling of the global cobalt extraction, supply, price and

depletion of extractable resources using the world6 model. BioPhys. Econ. Resour. Qual. **2**(1), 4 (2017). https://doi.org/10.1007/s41247-017-0017-0

12. S. Bastian, W. Busch, D. Kühnel, A. Springer, T. Meißner et al., Toxicity of tungsten carbide and cobalt-doped tungsten carbide nanoparticles in mammalian cells in vitro. Environ. Health Perspect. **117**(4), 530 (2009). https://doi.org/10.1289/ehp.0800121

13. IARC Working Group on the Evaluation of Carcinogenic Risks to Humans, Cobalt in hard metals and cobalt sulfate, gallium arsenide, indium phosphide and vanadium pentoxide. IARC monographs on the evaluation of carcinogenic risks to humans **86**, 1 (2006)

14. Y. Kanemitsu, T. Nishimura, H. Yoshino, K. Takao, Y. Masumoto, Effect of hot isostatic pressing on binderless cemented carbide. Int. J. Refract. Met. Hard Mater. **1**(2), 66–68 (1982)

15. M.F. Ashby, *The CES EduPack Resource Booklet 2: Material and Process Selection Charts* (Granta Design Limited, Cambridge, 2009)

16. K.M. Tsai, C.Y. Hsieh, H.H. Lu, Sintering of binderless tungsten carbide. Ceram. Int. **36**(2), 689–692 (2010). https://doi.org/10.1016/j.ceramint.2009.10.017

17. J. Poetschke, V. Richter, T. Gestrich, Sintering behaviour of binderless tungsten carbide, in *Euro PM2012 Congress and Exhibition*, Basel, pp. 7–12, September 2012

18. D.J. Ma, Z.L. Kou, Y.J. Liu, Y.K. Wang, S.P. Gao et al., Submicron binderless tungsten carbide sintering behavior under high pressure and high temperature. Int. J. Refract. Met. Hard Mater. **54**, 427–432 (2016). https://doi.org/10.1016/j.ijrmhm.2015.10.001

19. D. Demirskyi, A. Ragulya, D. Agrawal, Initial stage sintering of binderless tungsten carbide powder under microwave radiation. Ceram. Int. **37**(2), 505–512 (2011). https://doi.org/10.1016/j.ceramint.2010.09.036

20. R.L. Coble, Sintering crystalline solids. I. Intermediate and final state diffusion models. J. Appl. Phys. **32**(5), 787–792 (1961). https://doi.org/10.1063/1.1736107

21. R.L. Coble, Sintering crystalline solids. II. Experimental test of diffusion models in powder compacts. J. Appl. Phys. **32**(5), 793–799 (1961). https://doi.org/10.1063/1.1736108

22. P. Boch, A. Leriche, Sintering and Microstructure of Ceramics, in *Ceramic Materials: Processes, Properties, and Applicatons*, ed. by P. Boch, J.C. Niepce (ISTE Ltd, New Porth Beach, 2007), pp. 55–94. https://doi.org/10.1002/9780470612415.ch3

23. C. Agte, R. Kohlermann, Hilfsmetallarme Hartmetallegierungen. Die Tech. **10**, 686–689 (1957)

24. T. Ungár, A. Borbély, G.R. Goren-Muginstein, S. Berger, A.R. Rosen, Particle-size, size distribution and dislocations in nanocrystalline tungsten-carbide. Nanostruct. Mater. **11**(1), 103–113 (1911). https://doi.org/10.1016/S0965-9773(99)00023-9

25. V. Richter, G. Boden, M. Nebelung, M. Ruthendorf, Manufacturing and properties of superhard materials with ceramic

sintering aids. *Presentation of the COST503-3rd Round Annual Meeting, Subgroup Hard Materials*, Hannover (1994)

26. V. Richter, Hard sintered materials made of nano-sized powders. Annual Report of Fraunhofer IKTS, pp. 44–45 (1995)

27. V. Richter, Manufacturing and properties of super-ultrafine hardmetals. Annual Report of Fraunhofer IKTS, pp. 46–47 (1997)

28. Editors of JOM, European powder metallurgy association awards innovation. J. Miner. Met. Mater. Soc. **53-3**, 4–9 (2001)

29. V. Richter, M. Ruthendorf, Wasserstrahlschneidhochdruckdüse. DE Patent No. 10052021 (2000)

30. J. Gurland, A study of the effect of carbon content on the structure and properties of sintered WC–Co alloys. Trans. AIME **200**(3), 285–290 (1954)

31. C.M. Fernandes, A.M.R. Senos, Cemented carbide phase diagrams: a review. Int. J. Refract. Met. Hard Mater. **29**(4), 405–418 (2011). https://doi.org/10.1016/j.ijrmhm.2011.02.004

32. S.K. Li, J.Q. Li, Y. Li, F.S. Liu, W.Q. Ao, Dense pure binderless WC bulk material prepared by spark plasma sintering. Mater. Sci. Technol. **31**(14), 1749–1756 (2015). https://doi.org/10.1179/1743284714Y.0000000753

33. A. Gubernat, P. Rutkowski, G. Grabowski, D. Zientara, Hot pressing of tungsten carbide with and without sintering additives. Int. J. Refract. Met. Hard Mater. **43**, 193–199 (2014). https://doi.org/10.1016/j.ijrmhm.2013.12.002

34. A. Gubernat, L. Stobierski, Fractography of dense metallike carbides sintered with carbon. Key Eng. Mater. **409**, 287–290 (2009). https://doi.org/10.4028/www.scientific.net/KEM.409.287

35. J. Poetschke, V. Richter, T. Gestrich, A. Michaelis, Grain growth during sintering of tungsten carbide ceramics. Int. J. Refract. Met. Hard Mater. **43**, 309–316 (2014). https://doi.org/10.1016/j.ijrmhm.2014.01.001

36. R.T. Fox, R. Nilsson, Binderless tungsten carbide carbon control with pressureless sintering. Int. J. Refract. Met. Hard Mater. **76**, 82–89 (2018). https://doi.org/10.1016/j.ijrmhm.2018.05.020

37. A. Nino, K. Morimura, S. Sugiyama, H. Taimatsu, Effects of C and NbC additions on the microstructure and mechanical properties of binderless WC ceramics. Key Eng. Mater. **749**, 205–210 (2017). https://doi.org/10.4028/www.scientific.net/KEM.749.205

38. A. Nino, K. Takahashi, S. Sugiyama, H. Taimatsu, Effects of carbon addition on microstructures and mechanical properties of binderless tungsten carbide. Mater. Trans. **53**(8), 1475–1480 (2012). https://doi.org/10.2320/matertrans.M2012148

39. G.Z. Zhang, C. Wang, J.X. Zhang, M.L. Zhou, T.X. Zhou, Effects of mixed carbon content on spark plasma sintering of binder-free nanostructured WC cemented carbides. Rare Metals Cemented Carbides **33**(2), 12–15 (2005)

40. L. Girardini, M. Zadra, F. Casari, A. Molinariet, SPS, binderless WC powders, and the problem of sub carbide. Metal Powder Rep. **63**(4), 18–22 (2008). https://doi.org/10.1016/S0026-0657(09)70039-6

41. S.I. Cha, S.H. Hong, Microstructures of binderless tungsten carbides sintered by spark plasma sintering process. Mater. Sci. Eng., A **356**(1–2), 381–389 (2003). https://doi.org/10.1016/S0921-5093(03)00151-5

42. J.F. Zhao, T. Holland, C. Unuvar, Z.A. Munir, Sparking plasma sintering of nanometric tungsten carbide. Int. J. Refract. Met. Hard Mater. **27**(1), 130–139 (2009). https://doi.org/10.1016/j.ijrmhm.2008.06.004

43. K. Kornaus, M. Rączka, A. Gubernat, D. Zientara, Pressureless sintering of binderless tungsten carbide. J. Eur. Ceram. Soc. **37**(15), 4567–4576 (2017). https://doi.org/10.1016/j.jeurceramsoc.2017.06.008

44. Z.Z. Fang, H. Wang, Densification and grain growth during sintering of nanosized particles. Int. Mater. Rev. **53**(6), 326–352 (2008). https://doi.org/10.1179/174328008X353538

45. J. Poetschke, V. Richter, A. Michaelis, Fundamentals of sintering nanoscaled binderless hardmetals. Int. J. Refract. Met. Hard Mater. **49**, 124–132 (2015). https://doi.org/10.1016/j.ijrmhm.2014.04.022

46. M.J. Mayo, Processing of nanocrystalline ceramics from ultrafine particles. Int. Mater. Rev. **41**(3), 85–115 (1996). https://doi.org/10.1179/imr.1996.41.3.85

47. C.C. Koch, *Nanostructured Materials: Processing, Properties and Applications* (Noyes Publications, New York, 2002), pp. 173–217

48. A.N. Kumar, M. Watabe, K. Kurokawa, The sintering kinetics of ultrafine tungsten carbide powders. Ceram. Int. **37**(7), 2643–2654 (2011). https://doi.org/10.1016/j.ceramint.2011.04.011

49. S. Berger, R. Porat, R. Rosen, Nanocrystalline materials: a study of WC-based hard metals. Prog. Mater Sci. **42**(1–4), 311–320 (1997). https://doi.org/10.1016/S0079-6425(97)00021-2

50. Z.Z. Fang, X. Wang, T. Ryu, K.S. Hwang, H.Y. Sohn, Synthesis, sintering, and mechanical properties of nanocrystalline cemented tungsten carbide—a review. Int. J. Refract. Met. Hard Mater. **27**(2), 288–299 (2009). https://doi.org/10.1016/j.ijrmhm.2008.07.011

51. K. Brookes, Nano carbides make for low temperature sintering. Metal Powder Rep. **64**(9), 26–32 (2009). https://doi.org/10.1016/S0026-0657(09)70217-6

52. M. Leiderman, O. Botstein, A. Rosen, Sintering microstructure and properties of sub-micron cemented carbide. Powder Metall. **40**, 219 (1997). https://doi.org/10.1179/pom.1997.40.3.219

53. R. Porat, S. Berger, A. Rosen, Dilatometric study of the sintering mechanism of nanocrystalline cemented carbides. Nanostruct. Mater. **7**(4), 429–436 (1996). https://doi.org/10.1016/0965-9773(96)00014-1

54. H. Ogawa, Y. Kataoka, Observation of sintering of several cemented carbides by a new high-temperature sintering dilatometer. High Temp.-High Press. **13**(5), 481–494 (1981)

55. G.R. Goren-Muginstein, S. Berger, A. Rosen, Sintering studies of nanocrystalline WC powder, in *Proceedings of the 14th International Plansee Seminar*, Metallwerk Plansee, Reutte, February 1997

56. H.C. Kim, I.J. Shon, J.E. Garay, Z.A. Munir, Consolidation and properties of binderless sub-micron tungsten carbide by field-activated sintering. Int. J. Refract. Met. Hard Mater. **22**(6), 257–264 (2004). https://doi.org/10.1016/j.ijrmhm.2004.08.003

57. V.N. Chuvil'deev, Y.V. Blagoveshchenskiy, A.V. Nokhrin, M.S. Boldin, N.V. Sakharov et al., Spark plasma sintering of tungsten carbide nanopowders obtained through DC arc plasma synthesis. J. Alloy. Compd. **708**, 547–561 (2017). https://doi.org/10.1016/j.jallcom.2017.03.035

58. V.N. Chuvil'deev, Y.V. Blagoveshchenskiy, A.V. Nokhrin, N.V. Sakharov, M.S. Boldin et al., Sparking plasma sintering of tungsten carbide nanopowders. Nanotechnol. Russ. **10**(5–6), 434–448 (2015). https://doi.org/10.1134/S1995078015030040

59. B.W. Kwak, J.K. Yoon, I.J. Shon, Pulsed current activated rapid sintering of binderless nanostructured TiC and WC and their properties. J. Nanosci. Nanotechnol. **17**(6), 4214–4217 (2017). https://doi.org/10.1166/jnn.2017.13388

60. I.J. Shon, Mechanical properties and rapid sintering of binderless nanostructured TiC and WC by high frequency induction heated sintering. J. Ceram. Process. Res. **17**(7), 707–711 (2016)

61. I.J. Shon, B.R. Kim, J.M. Doh, J.K. Yoon, K.D. Woo, Properties of nanostructured tungsten carbide and their rapid consolidation by pulsed current activated sintering. Phys. Scripta **T139**, 014043 (2010). https://doi.org/10.1088/0031-8949/2010/T139/014043

62. G.R. Goren-Muginstein, S. Berger, A. Rosen, Sintering study of nanocrystalline tungsten carbide powders. Nanostruct. Mater. **10**(5), 795–804 (1998). https://doi.org/10.1016/S0965-9773(98)00116-0

63. X.Y. Ren, Z.J. Peng, C.B. Wang, Z.Q. Fu, L.H. Qi et al., Effect of ZrC nano-powder addition on the microstructure and mechanical properties of binderless tungsten carbide fabricated by spark plasma sintering. Int. J. Refract. Met. Hard Mater. **48**, 398–407 (2015). https://doi.org/10.1016/j.ijrmhm.2014.10.013

64. K. Biswas, A. Mukhopadhyay, B. Basu, K. Chattopadhyay, Densification and microstructure development in spark plasma sintered WC–6 wt% ZrO_2 nanocomposites. J. Mater. Res. **22**(6), 1491–1501 (2007). https://doi.org/10.1557/JMR.2007.0189

65. B. Basu, J.H. Lee, D.Y. Kim, Development of WC–ZrO_2 nanocomposites by spark plasma sintering. J. Am. Ceram. Soc. **87**(2), 317–319 (2004). https://doi.org/10.1111/j.1551-2916.2004.00317.x

66. R. Holm, *Electric Contacts: Theory and Application* (Springer, New York, 1967), p. 22. https://doi.org/10.1007/978-3-662-06688-1

67. G. Petzow, W.A. Kaysser, Sintering with additives, in *Sintering Key Papers*, ed. by S. Somiya, Y. Moriyoshi (Elsevier, London, 1990), pp. 615–638. https://doi.org/10.1007/978-94-009-0741-6_39

68. J.L. Sun, J. Zhao, M.J. Chen, X.C. Wang, X. Zhong et al., Determination of microstructure and mechanical properties of functionally graded WC–TiC–Al$_2$O$_3$–GNPs micro-nano composite tool materials via two-step sintering. Ceram. Int. **43**(12), 9276–9284 (2017). https://doi.org/10.1016/j.ceramint.2017.04.086

69. Z. Qiao, J. Räthel, L.M. Berger, M. Herrmann, Investigation of binderless WC–TiC–Cr$_3$C$_2$ hard materials prepared by spark plasma sintering (SPS). Int. J. Refract. Met. Hard Mater. **38**, 7–14 (2013). https://doi.org/10.1016/j.ijrmhm.2012.12.002

70. Z. Li, S. Cheng, C. Shu, N. Qing, C. Xin et al., Hot pressing densification and grain growth behavior of WC–TiC–TaC binderless carbide. Mater. Sci. Eng. Powder Metall. **16**(5), 781–786 (2011)

71. A. Nino, Y. Izu, T. Sekine, S. Sugiyama, H. Taimatsu, Effects of ZrC and SiC addition on the microstructures and mechanical properties of binderless WC. Int. J. Refract. Met. Hard Mater. **69**, 259–265 (2017). https://doi.org/10.1016/j.ijrmhm.2017.09.002

72. A. Nino, N. Takahashi, S. Sugiyama, H. Taimatsu, Effects of carbide grain growth inhibitors on the microstructures and mechanical properties of WC–SiC–Mo$_2$C hard ceramics. Int. J. Refract. Met. Hard Mater. **43**, 150–156 (2014). https://doi.org/10.1016/j.ijrmhm.2013.11.016

73. A. Fazili, L. Nikzad, M.R. RahimiPour, M. Razavi, E. Salahi, Effect of Al$_2$O$_3$ ceramic binder on mechanical and microstructure properties of spark plasma sintered WC–Co cermets. Int. J. Refract. Met. Hard Mater. **69**, 189–195 (2017). https://doi.org/10.1016/j.ijrmhm.2017.08.010

74. A. Vornberger, J. Pötschke, C. Berger, Manufacturing and properties of tungsten carbide-oxide composites. Key Eng. Mater. **742**, 223–230 (2017). https://doi.org/10.4028/www.scientific.net/KEM.742.223

75. J. Wang, D. Zuo, L. Zhu, W.W. Li, Z.B. Tu et al., Effects and influence of Y$_2$O$_3$ addition on the microstructure and mechanical properties of binderless tungsten carbide fabricated by spark plasma sintering. Int. J. Refract. Met. Hard Mater. **71**, 167–174 (2018). https://doi.org/10.1016/j.ijrmhm.2017.11.016

76. O.A. El-Kady, Effect of nano-yttria addition on the properties of WC/Co composites. Mater. Des. **52**, 481–486 (2013). https://doi.org/10.1016/j.matdes.2013.05.034

77. X.Y. Ren, Z.J. Peng, C. Wang, H.Z. Miao, Influence of nano-sized La$_2$O$_3$ addition on the sintering behavior and mechanical properties of WC–La$_2$O$_3$ composites. Ceram. Int. **41**(10), 14811–14818 (2015). https://doi.org/10.1016/j.ceramint.2015.08.002

78. A. Rajabi, M.J. Ghazali, A.R. Daud, Chemical composition, microstructure and sintering temperature modifications on mechanical properties of TiC-based cerme—a review. Mater. Des. **67**, 95–106 (2017). https://doi.org/10.1016/j.matdes.2014.10.081

79. H. Kim, D. Kim, I. Ko et al., Sintering behavior and mechanical properties of binderless WC–TiC produced by pulsed current activated sintering. J. Ceram. Process Res. **8**(2), 91 (2007)

80. S. Imasato, K. Tokumoto, T. Kitada, S. Sakaguchi, Properties of ultra-fine grain binderless cemented carbide 'RCCFN'. Int. J. Refract. Met. Hard Mater. **13**(5), 305–312 (1995). https://doi.org/10.1016/0263-4368(95)92676-B

81. H.C. Kim, D.K. Kim, K.D. Woo, I.Y. Ko, I.J. Shon, Consolidation of binderless WC–TiC by high frequency induction heating sintering. Int. J. Refract. Met. Hard Mater. **26**(1), 48–54 (2008). https://doi.org/10.1016/j.ijrmhm.2007.01.006

82. J.J. Gao, L.K. Jiang, J.P. Song, G.X. Liang, J. Ang et al., Effects of TiC content on microstructure and mechanical property of WC–TiC–TaC cemented carbides. J. Inorg. Mater. **32**(8), 891–896 (2017). https://doi.org/10.15541/jim20160633

83. H. Engqvist, G.A. Botton, N. Axe, S. Hogmark, A study of grain boundaries in a binderless cemented carbide. Int. J. Refract. Met. Hard Mater. **16**(4–6), 309–313 (1998). https://doi.org/10.1016/S0263-4368(98)00034-1

84. S.G. Huang, K. Vanmeensel, B. Vander, J. Vleugels, Binderless WC and WC–VC materials obtained by pulsed electric current sintering. Int. J. Refract. Met. Hard Mater. **26**(1), 41–47 (2008). https://doi.org/10.1016/j.ijrmhm.2007.01.002

85. H.C. Kim, H.K. Park, I.K. Jeong, I.Y. Ko, I.J. Shon, Sintering of binderless WC–Mo$_2$C hard materials by rapid sintering process. Ceram. Int. **34**(6), 1419–1423 (2008). https://doi.org/10.1016/j.ceramint.2007.03.029

86. H. Taimatsu, S. Sugiyama, M. Komatsu, Effects of Cr$_3$C$_2$ and V$_8$C$_7$ on the microstructure and mechanical properties of WC–SiC whisker ceramics. Mater. Trans. **50**(10), 2435–2440 (2009). https://doi.org/10.2320/matertrans.M2009169

87. A. Nino, Y. Nakaibayashi, S. Sugiyama, H. Taimatsu, Microstructure and mechanical properties of WC–SiC composites. Mater. Trans. **52**(8), 1641–1645 (2011). https://doi.org/10.2320/matertrans.M2011045

88. S. Sugiyama, D. Kudo, H. Taimatsu, Preparation of WC–SiC whisker composites by hot pressing and their mechanical properties. Mater. Trans. **49**(7), 1644–1649 (2008). https://doi.org/10.2320/matertrans.MRA2008019

89. A. Nino, Y. Nakaibayashi, S. Sugiyama, H. Taimatsu, Effect of Mo$_2$C addition on the microstructures and mechanical properties of WC–SiC ceramics. Int. J. Refract. Met. Hard Mater. **64**, 35–39 (2017). https://doi.org/10.1016/j.ijrmhm.2016.12.018

90. A. Nino, T. Sekine, K. Sugawara, S. Sugiyama, H. Taimatsu, Effect of added Cr$_3$C$_2$ on the microstructure and mechanical properties of WC–SiC ceramics. Key Eng. Mater. **656**, 33 (2015). https://doi.org/10.4028/www.scientific.net/KEM.656-657.33

91. O.L. Ighodaro, O.I. Okoli, Fracture toughness enhancement for alumina systems, a review. Int. J. Appl. Ceram. Technol. **5**(3), 313–323 (2008). https://doi.org/10.1111/j.1744-7402.2008.02224.x

92. W.H. Chen, H.T. Lin, P.K. Nayak, J.L. Huang, Material properties of tungsten carbide–alumina composites fabricated by

spark plasma sintering. Ceram. Int. **40**(9), 15007–15012 (2014). https://doi.org/10.1016/j.ceramint.2014.06.102

93. W. Dong, S. Zhu, Y. Wang, T. Bai, Influence of VC and Cr_3C_2 as grain growth inhibitors on WC–Al_2O_3 composites prepared by hot press sintering. Int. J. Refract. Met. Hard Mater. **45**, 223–229 (2014). https://doi.org/10.1016/j.ijrmhm.2014.04.011

94. W. Dong, S. Zhu, T. Bai, Y. Luo, Influence of Al_2O_3 whisker concentration on mechanical properties of WC–Al_2O_3 whisker composite. Ceram. Int. **41**(10), 13685–13691 (2015). https://doi.org/10.1016/j.ceramint.2015.07.167

95. H. Qu, S. Zhu, Two step hot pressing sintering of dense fine grained WC–Al_2O_3 composites. Ceram. Int. **39**(5), 5415–5425 (2013). https://doi.org/10.1016/j.ceramint.2012.12.049

96. W.H. Chen, H.T. Lin, P.K. Nayak, M.P. Chang, J.L. Huang et al., Sintering behavior and mechanical properties of WC–Al_2O_3 composites prepared by spark plasma sintering (SPS). Int. J. Refract. Met. Hard Mater. **48**, 414–417 (2015). https://doi.org/10.1016/j.ijrmhm.2014.10.016

97. W.W. Dong, S.G. Zhu, C.X. Ouyang, The effect of VC on the sintering ability and microstructure of WC–Al_2O_3 composites. Appl. Mech. Mater. **490**, 43–48 (2014). https://doi.org/10.4028/www.scientific.net/AMM.490-491.43

98. S.G. Zhu, H.X. Qu, C.X. Ouyang, Hot pressing of tungsten carbide ceramic matrix composites, in *Advances in Ceramic Matrix Composites*, ed. by I.M. Low (Woodhead Publishing, Cambridge, 2014), pp. 203–229. https://doi.org/10.1016/B978-0-08-102166-8.00009-8

99. D. Zheng, X. Li, X. Ai, C. Yang, Y. Li, Bulk WC–Al_2O_3 composites prepared by spark plasma sintering. Int. J. Refract. Met. Hard Mater. **30**(1), 51–56 (2012). https://doi.org/10.1016/j.ijrmhm.2011.07.003

100. S.J. Oh, B.S. Kim, J.K. Yoon, K.T. Hong, I.J. Shon, Enhanced mechanical properties and consolidation of the ultra-fine WC–Al_2O_3 composites using pulsed current activated heating. Ceram. Int. **42**(7), 9304–9310 (2016). https://doi.org/10.1016/j.ceramint.2016.02.113

101. H. Qu, S. Zhu, Q. Li, C. Quyang, Microstructure and mechanical properties of hot-pressing sintered WC–x vol.% Al_2O_3 composites. Mater. Sci. Eng., A **543**, 96–103 (2012). https://doi.org/10.1016/j.msea.2012.02.053

102. S.J. Oh, B.S. Kim, I.J. Shon, Mechanical properties and rapid consolidation of nanostructured WC and WC–Al_2O_3 composites by high-frequency induction-heated sintering. Int. J. Refract. Met. Hard Mater. **58**, 189–195 (2016). https://doi.org/10.1016/j.ijrmhm.2016.04.016

103. W.H. Tuan, R.Z. Chen, T.C. Wang, C.H. Cheng, P.S. Kuo, Mechanical properties of Al_2O_3/ZrO_2 composites. J. Eur. Ceram. Soc. **22**(16), 2827–2833 (2002). https://doi.org/10.1016/S0955-2219(02)00043-2

104. D. Zheng, X. Li, Y. Li, S. Qu, C. Yang, ZrO_2 (3Y) toughened WC composites prepared by spark plasma sintering. J. Alloy. Compd. **572**, 62–67 (2013). https://doi.org/10.1016/j.jallcom.2013.03.259

105. F.Z. Yang, J. Zhao, X. Ai, Effect of initial particulate and sintering temperature on mechanical properties and microstructure of WC–ZrO_2–VC ceramic composites. J. Mater. Process. Technol. **209**(9), 4531–4536 (2009). https://doi.org/10.1016/j.jmatprotec.2008.10.027

106. T. Venkateswaran, D. Sarkar, B. Basu, WC–ZrO_2 composites, processing and unlubricated tribological properties. Wear **260**(1–2), 1–9 (2006). https://doi.org/10.1016/j.wear.2004.11.005

107. T. Venkateswaran, D. Sarkar, B. Basu, Tribological properties of WC–ZrO_2 nanocomposites. J. Am. Ceram. Soc. **88**(3), 691–697 (2005). https://doi.org/10.1111/j.1551-2916.2005.00129.x

108. B. Basu, J.H. Lee, D.Y. Kim, Development of WC–ZrO_2 nanocomposites by spark plasma sintering. J. Am. Ceram. Soc. **87**(2), 317–319 (2004). https://doi.org/10.1111/j.1551-2916.2004.00317.x

109. O. Malek, B. Lauwers, Y. Perez, P.D. Baets, J. Vleugels, Processing of ultrafine ZrO_2 toughened WC composites. J. Eur. Ceram. Soc. **29**(16), 3371–3378 (2009). https://doi.org/10.1016/j.jeurceramsoc.2009.07.013

110. A. Nasser, M.A. Kassem, A. Elsayed, M.A. Gepreel, A.A. Moniem, Influence of grain refinement on microstructure and mechanical properties of tungsten carbide/zirconia nanocomposites. J. Mater. Eng. Perform. **25**(11), 5065–5075 (2016). https://doi.org/10.1007/s11665-016-2341-8

111. B. Basu, T. Venkateswaran, D. Sarkar, Pressureless sintering and tribological properties of WC–ZrO_2 composites. J. Eur. Ceram. Soc. **25**(9), 1603–1610 (2005). https://doi.org/10.1016/j.jeurceramsoc.2004.05.021

112. A. Mukhopadhyay, B. Basu, Consolidation–microstructure–property relationships in bulk nanoceramics and ceramic nanocomposites, a review. Int. Mater. Rev. **52**(5), 257–288 (2007). https://doi.org/10.1179/174328007X160281

113. Z.A. Munir, U. Anselmi-Tamburini, M. Ohyanagi, The effect of electric field and pressure on the synthesis and consolidation of materials, a review of the spark plasma sintering method. J. Mater. Sci. **41**(3), 763–777 (2006). https://doi.org/10.1007/s10853-006-6555-2

114. K. Inoue, US Patent, No 3 241 956 (1966)

115. M. Omori, Sintering, consolidation, reaction and crystal growth by the spark plasma system (SPS). Mater. Sci. Eng., A **287**(2), 183–188 (2000). https://doi.org/10.1016/S0921-5093(00)00773-5

116. R.S. Mishra, S.H. Risbud, A.K. Mukherjee, Influence of initial crystal structure and electrical pulsing on densification of nanocrystalline alumina powder. J. Mater. Res. **13**(1), 86–89 (1998). https://doi.org/10.1557/JMR.1998.0013

117. K.A. Khalil, Advanced sintering of nano-ceramic materials, in *Ceramic Materials-Progress in Modern Ceramics*, ed. by S. Feng (InTech, Shanghai, 2012), pp. 65–82

118. M. Suárez, J.L. Fernández, R. Menéndez, R. Torrecillas, H.U. Kessel et al., Challenges and opportunities for spark plasma sintering, a key technology for a new generation of materials,

in *Sintering Applications*, ed. by B. Ertuğ (InTech, Turkey, 2013), pp. 319–342. https://doi.org/10.5772/53706

119. B. Huang, L.D. Chen, S.Q. Bai, Bulk ultrafine binderless WC prepared by spark plasma sintering. Scr. Mater. **54**(3), 441–445 (2006). https://doi.org/10.1016/j.scriptamat.2005.10.014

120. S.I. Cha, S.H. Hong, B.K. Kim, Spark plasma sintering behavior of nanocrystalline WC–10Co cemented carbide powders. Mater. Sci. Eng., A **351**(1–2), 31–38 (2003). https://doi.org/10.1016/S0921-5093(02)00605-6

121. Y. Wang, D. Zhu, X. Jiang, P. Sun, Binderless sub-micron WC consolidated by hot pressing and treated by hot isostatic pressing. J. Ceram. Soc. Jpn. **122**(1425), 329–335 (2014). https://doi.org/10.2109/jcersj2.122.329

122. K.M. Tsai, The effect of consolidation parameters on the mechanical properties of binderless tungsten carbide. Int. J. Refract. Met. Hard Mater. **29**(2), 188–201 (2011). https://doi.org/10.1016/j.ijrmhm.2010.10.006

123. J. Zhang, G. Zhang, S. Zhao, X. Song, Binder-free WC bulk synthesized by spark plasma sintering. J. Alloy. Compd. **479**(1–2), 427–431 (2009). https://doi.org/10.1016/j.jallcom.2008.12.151

124. S.K. Sun, Y.M. Kan, G.J. Zhang, Fabrication of nanosized tungsten carbide ceramics by reactive spark plasma sintering. J. Am. Ceram. Soc. **94**(10), 3230–3233 (2011). https://doi.org/10.1111/j.1551-2916.2011.04813.x

125. M. Dopita, A. Salomon, D. Chmelik, B. Reichel, Field assisted sintering technique compaction of ultrafine-grained binderless WC hard metals. Acta Phys. Pol., A **122**(3), 639 (2012). https://doi.org/10.12693/APhysPolA.122.639

126. H.T. Kim, J.S. Kim, Y.S. Kwon, Mechanical properties of binderless tungsten carbide by spark plasma sintering, in *Proceedings of the 9th Russian-Korean International Symposium on Science and Technology*, KORUS (2005)

127. X. Liu, L. Tao, H. Shao, Z. Guo, J. Luo et al., Consolidation and properties of ultrafine binderless cemented carbide by spark plasma sintering. Rare Met. **27**(3), 320–323 (2008). https://doi.org/10.1016/S1001-0521(08)60137-0

128. X. Xia, X. Li, J. Li, D. Zheng, Microstructure and characterization of WC–2.8 wt% Al_2O_3–6.8 wt%ZrO_2 composites produced by spark plasma sintering. Ceram. Int. **42**(12), 14182–14188 (2016). https://doi.org/10.1016/j.ceramint.2016.06.044

129. H.C. Kim, I.J. Shon, I.K. Jeong, I.Y. Ko, J.K. Yoon et al., Rapid sintering of ultrafine WC and WC–Co hard materials by high-frequency induction heated sintering and their mechanical properties. Met. Mater. Int. **13**(1), 39–45 (2007). https://doi.org/10.1007/BF03027821

130. I.J. Shon, B.R. Kim, J.M. Doh, J.K. Yoon, K.D. Woo, Properties and rapid consolidation of ultra-hard tungsten carbide. J. Alloy. Compd. **489**(1), L4–L8 (2010). https://doi.org/10.1016/j.jallcom.2009.09.040

131. H. Awaji, S.M. Choi, E. Yagi, Mechanisms of toughening and strengthening in ceramic-based nanocomposites. Mech. Mater. **34**(7), 411–422 (2002). https://doi.org/10.1016/S0167-6636(02)00129-1

132. M. Taya, S. Hayashi, A.S. Kobayashi, H.S. Yoon, Toughening of a particulate-reinforced ceramic-matrix composite by thermal residual stress. J. Am. Ceram. Soc. **73**(5), 1382–1391 (1990). https://doi.org/10.1111/j.1151-2916.1990.tb05209.x

133. B. Budiansky, J.C. Amazigo, A.G. Evans, Small-scale crack bridging and the fracture toughness of particulate-reinforced ceramics. J. Mech. Phys. Solids **36**, 167–187 (1988). https://doi.org/10.1016/S0022-5096(98)90003-5

134. M.S. El-Eskandarany, Fabrication of nanocrystalline WC and nanocomposite WC–MgO refractory materials at room temperature. J. Alloy. Compd. **296**(1–2), 175–182 (2000). https://doi.org/10.1016/S0925-8388(99)00508-3

135. J. Ma, S. Zhu, C. Ouyang, Two-step hot-pressing sintering of nanocomposite WC–MgO compacts. J. Eur. Ceram. Soc. **31**(10), 1927–1935 (2011). https://doi.org/10.1016/j.jeurceramsoc.2011.04.001

136. C. Ouyang, S. Zhu, H. Qu, VC and Cr_3C_2 doped WC–MgO compacts prepared by hot-pressing sintering. Mater. Des. **40**, 550–555 (2012). https://doi.org/10.1016/j.matdes.2012.04.030

137. M. Radajewski, C. Schimpf, L. Krüger, Study of processing routes for WC–MgO composites with varying MgO contents consolidated by FAST/SPS. J. Eur. Ceram. Soc. **37**(5), 2031–2037 (2017). https://doi.org/10.1016/j.jeurceramsoc.2017.01.005

138. J.L. Sun, J. Zhao, X.Y. Ni, F. Gong et al., Fabrication of dense nano-laminated tungsten carbide materials doped with Cr_3C_2/VC through two-step sintering. J. Eur. Ceram. Soc. **38**(9), 3096–3103 (2018). https://doi.org/10.1016/j.jeurceramsoc.2018.02.037

139. J.L. Sun, J. Zhao, M.J. Chen, X.Y. Ni, Z.L. Li et al., Determination of microstructure and mechanical properties of VC/Cr_3C_2 reinforced functionally graded WC–TiC–Al_2O_3 micro-nano composite tool materials via two-step sintering. J. Alloys Compd. **709**, 197–205 (2017). https://doi.org/10.1016/j.jallcom.2017.03.137

140. P.M. Kelly, L.F. Rose, The martensitic transformation in ceramics-its role in transformation toughening. Prog. Mater Sci. **47**(5), 463–557 (2002). https://doi.org/10.1016/S0079-6425(00)00005-0

141. R.H. Hannink, P.M. Kelly, B.C. Muddle, Transformation toughening in zirconia-containing ceramics. J. Am. Ceram. Soc. **83**(3), 461–487 (2000). https://doi.org/10.1111/j.1151-2916.2000.tb01221.x

142. B. Basu, Toughening of yttria-stabilised tetragonal zirconia ceramics. Int. Mater. Rev. **50**(4), 239–256 (2005). https://doi.org/10.1179/174328005X41113

143. P.F. Becher, Microstructural design of toughened ceramics. J. Am. Ceram. Soc. **74**(2), 255–269 (1991). https://doi.org/10.1111/j.1151-2916.1991.tb06872.x

144. A. Mukhopadhyay, D. Chakravarty, B. Basu, Spark plasma-sintered WC–ZrO_2–Co nanocomposites with high fracture toughness and strength. J. Am. Ceram. Soc. **93**(6), 1754–1763 (2010). https://doi.org/10.1111/j.1551-2916.2010.03685.x

145. J. Wang, R. Stevens, Zirconia-toughened alumina (ZTA) ceramics. J. Mater. Sci. **24**(10), 3421–3440 (1989). https://doi.org/10.1007/BF02385721

146. D. Zheng, X. Li, Y. Li, S. Qu, C. Yang, Zirconia-toughened WC with/without VC and Cr_3C_2. Ceram. Int. **40**(1), 2011–2016 (2014). https://doi.org/10.1016/j.ceramint.2013.07.111

147. M. Bengisu, O.T. Inal, Whisker toughening of ceramics, toughening mechanisms, fabrication, and composite properties. Annu. Rev. Mater. Sci. **24**(1), 83–124 (1994). https://doi.org/10.1146/annurev.ms.24.080194.000503

148. M. Bengisu, O.T. Inal, O. Tosyali, On whisker toughening in ceramic materials. Acta Metall. Mater. **39**(11), 2509–2517 (1991). https://doi.org/10.1016/0956-7151(91)90066-A

149. P.F. Becher, C.H. Hsueh, P. Angelini et al., Toughening behavior in whisker-reinforced ceramic matrix composites. J. Am. Ceram. Soc. **71**(12), 1050–1061 (1988). https://doi.org/10.1111/j.1151-2916.1988.tb05791.x

150. X.B. Li, C.M. Ke, N. Li, Progress in ceramic matrix composite by SiC whisker toughening. Mater. Rev. **21**(8), 394–397 (2007)

151. Y.J. Chao, J. Liu, Study of WC ceramic tool material by SiC whisker toughening. Rare Metals Cemented Carbides **33**(4), 13–16 (2005)

152. H. Taimatsu, S. Sugiyama, M. Komatsu, Effects of Cr_3C_2 and V_8C_7 on the microstructure and mechanical properties of WC–SiC whisker ceramics. Mater. Trans. **50**(10), 2435–2440 (2009). https://doi.org/10.2320/matertrans.M2009169

153. D. Zheng, X. Li, Y. Li, S. Qu, C. Yang, In-situ elongated β-Si_3N_4 grains toughened WC composites prepared by one/two-step spark plasma sintering. Mater. Sci. Eng., A **561**, 445–451 (2013). https://doi.org/10.1016/j.msea.2012.10.059

154. Y. Li, D. Zheng, X. Li, S. Qu, C. Yang, Cr_3C_2 and VC doped WC–Si_3N_4 composites prepared by spark plasma sintering. Int. J. Refract. Met. Hard Mater. **41**, 540–546 (2013). https://doi.org/10.1016/j.ijrmhm.2013.07.004

155. Y. Li, X. Li, D. Zheng, S. Qu, C. Yang, et al., Tungsten carbide composite material comprising aluminium oxide particles and silicon nitride whiskers and preparation process thereof. WO, WO/2013/020317 (2013)

156. R. Lakshminarayanan, D.K. Shetty, R.A. Cutler, Toughening of layered ceramic composites with residual surface compression. J. Am. Ceram. Soc. **79**(1), 79–87 (1996). https://doi.org/10.1111/j.1151-2916.1996.tb07883.x

157. G. Blugan, R. Dobedoe, M. Lugovy, S. Koebel, J. Kuebler, Si_3N_4–TiN based micro-laminates with rising R-curve behavior. Compos. Part B **37**(6), 459–465 (2006). https://doi.org/10.1016/j.compositesb.2006.02.013

158. M. Lugovy, V. Slyunyayev, N. Orlovskaya, G. Blugan, J. Kuebler et al., Apparent fracture toughness of Si_3N_4-based laminates with residual compressive or tensile stresses in surface layers. Acta Mater. **53**(2), 289–296 (2005). https://doi.org/10.1016/j.actamat.2004.09.022

159. S. Iijima, Helical microtubules of graphitic carbon. Nature **354**(6348), 56–58 (1998). https://doi.org/10.1038/354056a0

160. S.C. Tjong, *Carbon Nanotube Reinforced Composites, Metal and Ceramic Matrices* (Wiley, Hoboken, 2009), pp. 61–64. https://doi.org/10.1002/9783527626991

161. I.J. Shon, K.I. Na, B.R. Kim, I.Y. Ko, J.M. Doh et al., Mechanical properties and consolidation of nanostructured WC–CNT composites by high frequency induction heated sintering. Rev. Adv. Mater. Sci. **28**, 9–12 (2011)

162. T. Bai, Fabrication and properties of WC–Al_2O_3 cemented carbide reinforced by single-walled carbon nanotubes. Appl. Mech. Mater. **404**, 91–94 (2013). https://doi.org/10.4028/www.scientific.net/AMM.404.91

163. T. Bai, T. Xie, Fabrication and mechanical properties of WC–Al_2O_3 cemented carbide reinforced by CNTs. Mater. Chem. Phys. **201**, 113–119 (2017). https://doi.org/10.1016/j.matchemphys.2017.08.018

164. T. Bai, T. Xie, Influence of TiO_2 contents and sintering temperature on the microstructure and mechanical properties of WC–Al_2O_3 cemented carbide reinforced by multi-wall carbon nanotubes. J. Alloy. Compd. **745**, 562–568 (2018). https://doi.org/10.1016/j.jallcom.2018.02.233

165. J.H. Jang, I.H. Oh, J.W. Lim, H.K. Park, Fabrication and mechanical properties of binderless-WC and WC–CNT hard materials by pulsed current activated sintering method. J. Ceram. Process. Res. **18**(7), 477–482 (2017)

166. T. Cao, X. Li, J. Li, M. Zhang, H. Qiu, Effect of sintering temperature on phase constitution and mechanical properties of WC–1.0wt% carbon nanotube composites. Ceram. Int. **44**(1), 164–169 (2018). https://doi.org/10.1016/j.ceramint.2017.09.154

167. K.S. Novoselov, A.K. Geim, S. Morozov, D. Jiang, M.I. Katsnelson et al., Two-dimensional gas of massless dirac fermions in graphene. Nature **438**(7065), 197–200 (2005). https://doi.org/10.1038/nature04233

168. A.K. Geim, Graphene, status and prospects. Science **324**(5934), 1530–1534 (2009). https://doi.org/10.1126/science.1158877

169. O. Tapasztó, L. Tapasztó, M. Markó, F. Kern, R. Gadow et al., Dispersion patterns of graphene and carbon nanotubes in ceramic matrix composites. Chem. Phys. Lett. **511**(4–6), 340–343 (2011). https://doi.org/10.1016/j.cplett.2011.06.047

170. S. Stankovich, D.A. Dikin, G.H. Dommett, K.M. Kohlhaas, E.J. Zimney et al., Graphene-based composite materials. Nature **442**(7100), 282–286 (2006). https://doi.org/10.1038/nature04969

171. A. Nieto, D. Lahiri, A. Agarwal, Synthesis and properties of bulk graphene nanoplatelets consolidated by spark plasma sintering. Carbon **50**(11), 4068–4077 (2012). https://doi.org/10.1016/j.carbon.2012.04.054

172. A. Nieto, A. Bisht, D. Lahiri, C. Zhang, A. Agarwal, Graphene reinforced metal and ceramic matrix composites, a review. Int. Mater. Rev. **62**(5), 241–302 (2017). https://doi.org/10.1080/09506608.2016.1219481

173. I. Ahmad, M. Islam, T. Subhani, Y.Q. Zhou, Toughness enhancement in graphene nanoplatelet/SiC reinforced Al_2O_3 ceramic hybrid nanocomposites. Nanotechnology

27(42), 425704 (2016). https://doi.org/10.1088/0957-4484/27/42/425704

174. L.S. Walker, V.R. Marotto, M.A. Rafiee, N. Koratkar, E.L. Corral, Toughening in graphene ceramic composites. ACS Nano **5**(4), 3182–3190 (2011). https://doi.org/10.1021/nn200319d

175. M.S. Asl, M.G. Kakroudi, Characterization of hot-pressed graphene reinforced ZrB_2–SiC composite. Mater. Sci. Eng., A **625**, 385–392 (2015). https://doi.org/10.1016/j.msea.2014.12.028

176. J. Liu, H. Yan, M.J. Reece, K. Jiang, Toughening of zirconia/alumina composites by the addition of graphene platelets. J. Eur. Ceram. Soc. **32**(16), 4185–4193 (2012). https://doi.org/10.1016/j.jeurceramsoc.2012.07.007

177. A. Nieto, D. Lahiri, A. Agarwal, Graphene nano platelets reinforced tantalum carbide consolidated by spark plasma sintering. Mater. Sci. Eng., A **582**, 338–346 (2013). https://doi.org/10.1016/j.msea.2013.06.006

178. J.L. Sun, J. Zhao, M.J. Chen, Y.H. Zhou, X.Y. Ni et al., Multilayer graphene reinforced functionally graded tungsten carbide nano-composites. Mater. Des. **134**, 171–180 (2017). https://doi.org/10.1016/j.matdes.2017.08.041

179. W. Tang, L. Zhang, J.F. Zhu, Y. Chen, W. Tian et al., Effect of direct current patterns on densification and mechanical properties of binderless tungsten carbides fabricated by the spark plasma sintering system. Int. J. Refract. Met. Hard Mater. **64**, 90–97 (2017). https://doi.org/10.1016/j.ijrmhm.2017.01.010

180. J. Poetschke, V. Richter, A. Michaelis, Influence of small additions of MeC on properties of binderless tungsten carbide, in *Euro PM 2014 International Conference and Exhibition*, Salzburg, Austria, September 2014

181. M. Dopita, C.R. Sriram, D. Chmelik, A. Salomon, H.J. Seifert, Spark plasma sintering of nanocrystalline binderless WC hard metals, in *Proceedings of Conference Nanocon 2010*, Olomouc, Czech Republic. October 2010

182. H.C. Kim, J.K. Yoon, J.M. Doh, I.Y. Koa, I.J. Shon, Rapid sintering process and mechanical properties of binderless ultra fine tungsten carbide. Mater. Sci. Eng., A **435**, 717–724 (2006). https://doi.org/10.1016/j.msea.2006.07.127

183. H. Kim, D. Kim, I. Ko, I.J. Shon, Sintering behavior and mechanical properties of binderless WC–TiC produced by pulsed current activated sintering. J. Ceram. Process. Res. **8**(2), 91 (2007)

184. H. Engqvist, G.A. Botton, N. Axén et al., Microstructure and abrasive wear of binderless carbides. J. Am. Ceram. Soc. **83**(10), 2491–2496 (2000). https://doi.org/10.1111/j.1151-2916.2000.tb01580.x

185. J. Poetschke, V. Richter, R. Holke, Influence and effectivity of VC and Cr_3C_2 grain growth inhibitors on sintering of binderless tungsten carbide. Int. J. Refract. Met. Hard Mater. **31**, 218–223 (2012). https://doi.org/10.1016/j.ijrmhm.2011.11.006

186. X.Y. Ren, Z.J. Peng, Y. Peng, C.B. Wang, Z.Q. Fu et al., Ultrafine binderless WC-based cemented carbides with varied amounts of AlN nano-powder fabricated by spark plasma sintering. Int. J. Refract. Met. Hard Mater. **41**, 308–314 (2013). https://doi.org/10.1016/j.ijrmhm.2013.05.002

187. Y. Liu, Z. Wang, Q. Sun, B. Yin, J. Chen et al., Tribological behavior and wear mechanism of pure WC at wide range temperature from 25 to 800°C in vacuum and air environment. Int. J. Refract. Met. Hard Mater. **71**, 160–166 (2018). https://doi.org/10.1016/j.ijrmhm.2017.11.024

188. H. Engqvist, N. Axén, S. Hogmark, Resistance of a binderless cemented carbide to abrasion and particle erosion. Tribol. Lett. **4**(3–4), 251–258 (1998). https://doi.org/10.1023/A:1019132011439